AD-A158 806 ROLE OF ADDITIVES IN MINIMIZING ZINC ELECTRODE SHAPE CHANGE: THE EFFECT O.. (U) ALLIED CORP MORRISTOWN NJ L S MELNICKI ET AL. JUL 85 N00014-82-C-0701 1/1

UNCLASSIFIED F/G 7/4 NL

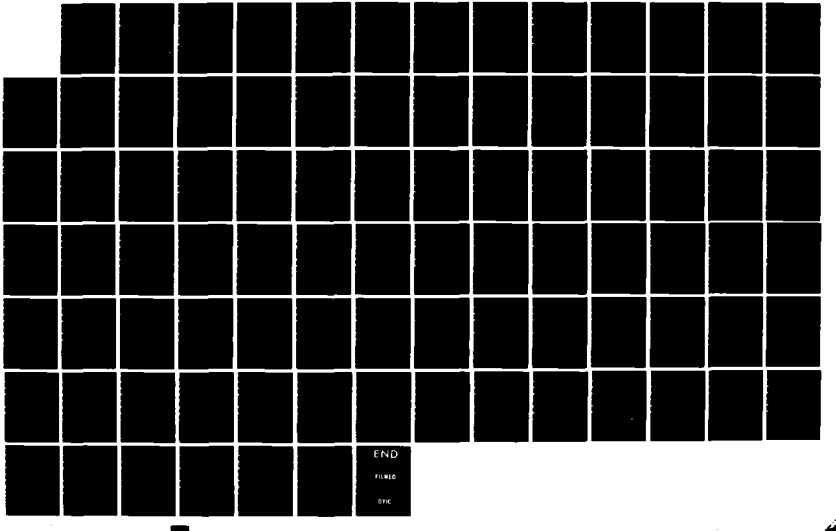

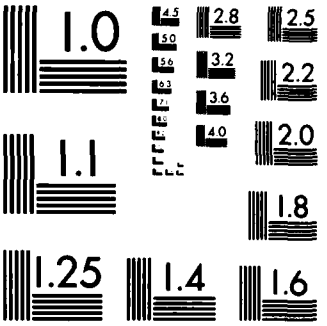

UNCLASSIFIED
SECURITY CLASSIFICATION

AD-A158 806

(2)

TATION PAGE

1a. REPORT SECURITY CLASSIFICATION UNCLASSIFIED	1b. RESTRICTIVE MARKINGS
2a. SECURITY CLASSIFICATION AUTHORITY	3. DISTRIBUTION / AVAILABILITY Approved for public release; Distribution Unlimited
2b. DECLASSIFICATION / DOWNGRADING SCHEDULE	UNCLASSIFIED/UNLIMITED
4. PERFORMING ORGANIZATION REPORT NUMBER(S) FINAL REPORT	5. MONITORING ORGANIZATION REPORT NUMBER(S)
6a. NAME OF PERFORMING ORGANIZATION ALLIED CORPORATION 6b. OFFICE SYMBOL (If applicable) CORP. TECH.	7a. NAME OF MONITORING ORGANIZATION OFFICE OF NAVAL RESEARCH
6c. ADDRESS (City, State, and ZIP Code) P.O. BOX 1021-R MORRISTOWN, NJ 07960	7b. ADDRESS (City, State, and ZIP Code) 800 NORTH QUNICY STREET ARLINGTON, VA 22217
8a. NAME OF FUNDING / SPONSORING ORGANIZATION OFFICE OF NAVAL RESEARCH 8b. OFFICE SYMBOL (If applicable) CODE 413	9. PROCUREMENT INSTRUMENT IDENTIFICATION NUMBER CONTRACT N00014-82-0701
8c. ADDRESS (City, State, and ZIP Code) 800 NORTH QUINCY STREET ARLINGTON, VA 22217	10. SOURCE OF FUNDING NUMBERS PROGRAM ELEMENT NO. / PROJECT NO. / TASK NO. / WORK UNIT ACCESSION NO

11 TITLE (Include Security Classification) ROLE OF ADDITIVES IN MINIMIZING ZINC ELECTRODE SHAPE CHANGE: THE EFFECT OF LEAD ON THE KINETICS OF Zn(II) REDUCTION IN CONCENTRATED ALKALINE MEDIA.

12 PERSONAL AUTHOR(S)
L. S. MELNICKI, I. LAZIC AND D. CIPRIS

13a. TYPE OF REPORT	13b. TIME COVERED	14. DATE OF REPORT (Year, Month, Day)	15. PAGE COUNT
TECHNICAL	FROM 9/20/82 TO 9/20/84	JULY 1985	

16 SUPPLEMENTARY NOTATION PRESENTED, IN PART, AT THE 35th MEETING OF INTERNATIONAL SOCIETY OF ELECTROCHEMISTRY, BERKELEY, CA, AUGUST 5-10, 1984, EXT. ABS. NO. 113-11.

17 COSATI CODES		
FIELD	GROUP	SUB-GROUP

18. SUBJECT TERMS (Continue on reverse if necessary and identify by block number)

19. ABSTRACT (Continue on reverse if necessary and identify by block number)

OVER

20. DISTRIBUTION / AVAILABILITY OF ABSTRACT ☒ UNCLASSIFIED/UNLIMITED ☐ SAME AS RPT. ☐ DTIC USERS	21. ABSTRACT SECURITY CLASSIFICATION UNCLASSIFIED
22a NAME OF RESPONSIBLE INDIVIDUAL D. CIPRIS	22b. TELEPHONE (Include Area Code) (201) 455-2880 22c. OFFICE SYMBOL

DD FORM 1473, 84 MAR 83 APR edition may be used until exhausted. All other editions are obsolete.

SECURITY CLASSIFICATION OF THIS PAGE
UNCLASSIFIED

19. ABSTRACT

The kinetics of zinc deposition in various media is among the most widely studied systems, along with hydrogen and oxygen reactions. The importance of the zinc electrode originates from the use of zinc as an anode material in commercially important primary and secondary batteries. The Ag-Zn battery, commercially available for a long time, has the highest practical energy and power densities among conventional secondary batteries. The Ni-Zn secondary battery is still under development. Both zinc electrodes operate in concentrated alkaline electrolytes.

In spite of the extensive number of studies, the mechanism of zinc reduction in alkaline media is not fully understood. The situation is further complicated in the presence of various metallic additives, which are commonly used in secondary alkaline batteries utilizing zinc anodes to suppress dendrite formation and/or facilitate uniform zinc deposition. Non-uniform zinc deposition leads to the phenomenon known as "zinc electrode shape change" in secondary batteries. The zinc electrode shape change is considered a leading factor in the premature loss of capacity of zinc batteries and to a generally unacceptably short cycle life.

The employment of metal additives remains largely empirical. Studies aimed at understanding the role of additives, conducted by various investigators, have produced controversial results. Without understanding the mechanism of additive action, the optimization of their effect on minimizing zinc electrode shape change is difficult to assess, if possible at all.

Of all the additives employed, lead appears to be the most commonly used in commercial practice, alone or in combination with other additives. Therefore, we have studied the effect of lead as an electrolyte additive on the kinetics of zinc deposition at solid electrodes (silver and zinc) in 45% KOH. A number of other additives claimed to be either beneficial or detrimental were studied to a lesser degree. For comparison, limited experiments with additives to pasted ZnO electrodes have also been conducted. The techniques used were cyclic voltammetry, chronopotentiometry and chronocoulometry.

A significant reduction in the rate of zinc deposition in the presence of lead was observed in all our experiments. We attribute this to co-deposition of lead, rather than a simple substrate effect. Our experimental evidence suggests that a dynamic layer-by-layer interaction of lead with zinc deposition plays the key role in the reduction of the deposition rate. The reduced deposition rate should lead to a more uniform zinc deposit, which in turn should lead to a reduced shape change upon cycling in practical cells. While further work is in order (especially on the dissolution process of zinc, which is also affected by lead) our results point to the possibility of employing electrolyte additives, as opposed to additives to the ZnO paste in practical cells.

During the course of this work we have employed a semidifferentiation algorithm for the analysis of chronocoulometric data for Zn (II) reduction in concentrated alkaline media. The chronocoulometric algorithm does not require an advanced knowledge of kinetic parameters and uses the entire data set for analysis, thus eliminating the need for approximation or for non-linear data fitting techniques. Kinetic data obtained in this work compare favorably with previously published results. This technique could be extended to study of systems other than zincate.

OFFICE OF NAVAL RESEARCH

Contract N00014-82-C-0701

FINAL TECHNICAL REPORT

ROLE OF ADDITIVES IN MINIMIZING ZINC ELECTRODE SHAPE CHANGE: THE EFFECT OF LEAD ON THE KINETICS OF Zn(II) REDUCTION IN CONCENTRATED ALKALINE MEDIA

BY

L. S. MELNICKI, I. LAZIC AND D. CIPRIS

Presented, in part,

at the 35th Meeting of International Society of Electrochemistry,

Berkeley, CA, August 5-10, 1984, Ext. Abs. No. 113-11

ALLIED CORPORATION, CORPORATE TECHNOLOGY
P.O. BOX 1021-R, MORRISTOWN, NJ 07960

July, 1985

1. ABSTRACT

The kinetics of zinc deposition in various media is among the most widely studied systems, along with hydrogen and oxygen reactions. The importance of the zinc electrode originates from the use of zinc as an anode material in commercially important primary and secondary batteries. The Ag-Zn battery, commercially available for a long time, has the highest practical energy and power densities among conventional secondary batteries. The Ni-Zn secondary battery is still under development. Both zinc electrodes operate in concentrated alkaline electrolytes.

In spite of the extensive number of studies, the mechanism of zinc reduction in alkaline media is not fully understood. The situation is further complicated in the presence of various metallic additives, which are commonly used in secondary alkaline batteries utilizing zinc anodes to suppress dendrite formation and/or facilitate uniform zinc deposition. Non-uniform zinc deposition leads to the phenomenon known as zinc electrode shape change in secondary batteries. The zinc electrode shape change is considered a leading factor in the premature loss of capacity of zinc batteries and to a generally unacceptably short cycle life.

The employment of metal additives remains largely empirical. Studies aimed at understanding the role of additives, conducted by various investigators, have produced controversial results. Without understanding the mechanism of additive action, the optimization of their effect on minimizing zinc electrode shape change is difficult to assess, if possible at all.

Of all the additives employed, lead appears to be the most commonly used in commercial practice, alone or in combination with other additives. Therefore, we have studied the effect of lead as an electrolyte additive on the kinetics of zinc deposition at solid electrodes (silver and zinc) in 45% KOH. A number of other additives claimed to be either beneficial or detrimental were studied to a lesser degree. For comparison, limited experiments with additives to pasted ZnO electrodes have also been conducted. The techniques used were cyclic voltammetry, chronopotentiometry and chronocoulometry.

A significant reduction in the rate of zinc deposition in the presence of lead was observed in all our experiments. We attribute this to co-deposition of lead, rather than a simple substrate effect. Our experimental evidence suggests that a dynamic layer-by-layer interaction of lead with zinc deposition plays the key role in the reduction of the deposition rate. The reduced deposition rate should lead to a more uniform zinc deposit, which in turn should lead to a reduced shape change upon cycling in practical cells. While further work is in order (especially on the dissolution process of zinc, which is also affected by lead) our results point to the possibility of employing electrolyte additives, as opposed to additives to the ZnO paste in practical cells.

During the course of this work we have employed a semidifferentiation algorithm for the analysis of chronocoulometric data for Zn (II) reduction in concentrated alkaline media. The chronocoulometric algorithm does not require an advanced knowledge of kinetic parameters and uses the entire data set for analysis, thus eliminating the need for approximation or for non-linear data fitting techniques. Kinetic data obtained in this work compare favorably with previously published results. This technique could be extended to study of systems other than zincate.

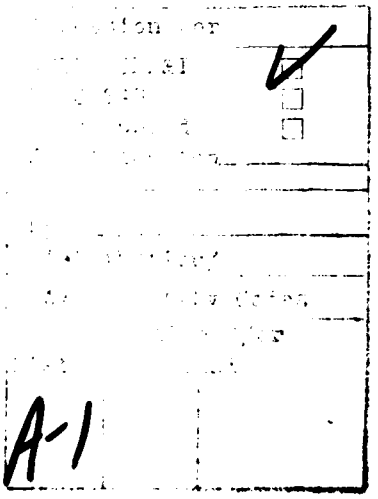

2. INTRODUCTION

Shape change of zinc electrodes is the major factor contributing to capacity loss and therefore to short cycle life of the Ag-Zn secondary battery. In spite of this drawback, the Ag-Zn cell has found extensive military application, since it has the highest practical energy and power densities among the conventional secondary batteries. Similarly, the commercialization of the Ni-Zn battery, aimed primarily at electric vehicle, but having also military importance, is largely hampered by the Zn shape problem. The solution of the Zn electrode shape change problem would thus benefit both military and civilian interests.

Several theories have been advanced in an effort to explain the shape change phenomenon (1). Consequently, various approaches have been used in an attempt to remedy the problem. The most successful, although still only partial remedy, appears to be the addition of small amounts of foreign metals (1 to 2%) to the Zn electrode, e.g., lead, cadmium, indium, or thallium, alone or in some combination. This approach is currently used in commercial Ag-Zn batteries.

The role of additives is little understood in spite of a fair amount of study. The employment of additives thus remains largely empirical. Without understanding the mechanisms of additives action, the optimization of their effect on minimizing Zn electrode shape change is difficult, if not impossible, to assess.

Earlier versions of commercial silver-zinc batteries contained HgO, mixed with zinc oxide paste (1 to 4%) to suppress hydrogen evolution. This practice has been discontinued for several reasons; in addition to

the high toxicity of Hg (which can cause severe problems in the case of battery shorting and possible fire), the presence of mercury is believed to accelerate the rate of zinc electrode shape change, resulting in rapid capacity loss (2). Substitutes for mercury were therefore sought.

Himy et al. (3) were the first to recommend the addition of PbO in combination with other metal oxide additives, such as CdO or Tl_2O_3, instead of HgO. The presence of PbO not only suppresses hydrogen evolution, but, more importantly, reduces the rate of zinc electrode shape change and consequently preserves the battery capacity through extended cycling. These experiments led to the employment of PbO and other mercury substitutes in commercial silver-zinc cells. The metallic additives are applied in the form of oxides (or other salts) and mixed with zinc oxide during manufacture of the Zn electrode. This method has the inherent disadvantage of possible nonuniformity of the resulting mixture.

The original, largely empirical work did not cast light on the mechanism by which reduction of the rate of shape change occurs. This work, however, prompted a series of investigations by others, aimed at understanding the nature of additive effects (4-7). The experiments were usually conducted in experimental Ni-Zn cells, with additives incorporated in the ZnO paste electrode. The conclusions reached are rather controversial.

McBreen et al. (4) studied the effect of HgO, Tl_2O_3, PbO, CdO, In_2O_3, $In(OH)_3$, In and Ga_2O_3 (alone or in combinations). Typical concentrations of additives in the ZnO paste were 1% PbO or SnO_2, with 0.5 to 2% of other metal oxides (weight percent). Expanded silver mesh was

used as a current collector. They observed that all the additives have an effect on the polarizability of the Zn electrode, some decreasing (Ga_2O_3, CdO, HgO) and some increasing (Tl_2O_3, PbO) the polarizability. In (and its salts) not only changed the slope (increased polarizability), but also altered the shape of the polarization curve. The morphology of Zn deposits was correspondingly affected. PbO and In or $In(OH_3)$ produce dense deposits, while Ga_2O_3 and CdO produce fine deposit structures, typical of Zn electrodes with no additives. Cycling experiments, for over 300 cycles, using a mixture of $In(OH)_3$ and PbO showed this combination "particularly effective in maintaining zinc electrode capacity with minimal shape change or bulging of the cell"(4). McBreen et al. attributed the observed beneficial effect of PbO (and some other additives) to the increased polarizability of the Zn electrode, which improves current distribution. Independent studies by McBreen have indicated non-uniform current distribution during the charging process, which could lead to shape change (8). Based on these results and a separate study of the effect metal substrates have on the morphology of Zn deposits (5,6), McBreen et al. concluded that the additive effect is a substrate effect.

Fletcher et al. (7) included a large number of additives in their studies of cell capacity and the rate of Zn electrode shape change. Additives studied included HgO, PbO, CdO, SnO_2, Bi_2O_3, TiO_2, V_2O_4, CeO_2, Fe_2O_3 and WO_3. The additives, in the form of metal oxides, were added to the ZnO paste in an experimental Ni-Zn cell. From the graphs of capacity vs. time they concluded that little or no influence was

exerted by any additive on the rate of shape change. However, all investigated additives, except WO_3, had a beneficial effect on the cell life. This was attributed to the inhibition of the growth of dendrites by additives. Overall, the best additives were found to be combinations of TiO_2(10%) plus HgO(2%) and CdO(5%) plus HgO(2%). The combinations CdO(5%), PbO(5%), HgO(2%) and SnO_2(5%), CdO(5%), HgO(2%) were claimed to be extremely effective for the prevention of dendrites, but capacity values were found to fluctuate greatly. Even though the best overall performance was claimed for combinations of additives, the article states that combinations of oxides were not better dendrite inhibitors than the individual oxides. In a subsequent paper, some of the same authors reported "statistically significant improvement" in the "cumulative capacity" (recorded at 100 cycles) of Ni-Zn test cells due to the addition of Bi_2O_3 to the ZnO paste electrode (9).

Effects of additives on the kinetics of Zn deposition/dissolution cannot be deduced from studies of pasted ZnO electrodes. Furthermore, the active mass is depleted of additives with cycling. It has been demonstrated that only a fraction of the original concentration remains after even relatively short cycling (10). The rate of depletion depends on the additive, but is always faster than the rate loss of zinc active material. Additives are lost to the separator, electrolyte, and zinc material detached from the electrode. Additives "lost" to the electrolyte could redeposit during the charging cycle, thus affecting the kinetics of the Zn(II) reduction reaction.

Of all the additives studied, lead appears to be the most commonly used in practice, either alone or in combination with other additives. Therefore, we have studied the effect of lead as an electrolyte additive on the kinetics of zinc deposition at solid electrodes (silver and zinc) in 45% KOH. A number of other additives claimed to be either beneficial or detrimental have been studied to a lesser degree: CdO, HgO, Bi_2O_3, Fe_2O_3, $In(OH)_3$, SnO, SnO_2, TiO_2, Tl_2O_3, V_2O_4 and WO_3. For comparison, limited experiments with additives to pasted ZnO electrodes have also been conducted. The techniques used were cyclic voltammetry, chronopotentiometry and chronocoulometry.

3. EXPERIMENTAL

Experiments were performed in a 200 ml borosilicate glass cell manufactured by Metrohm. The reference electrode consisted of a Hg/HgO electrode in 45% KOH constructed in the manner described by Thacker (11). All potentials are reported versus the Hg/HgO reference electrode. Zinc and silver disk electrodes were used as substrates for zinc deposition. Electrodes were fabricated from 2 mm rod inserted into Teflon™ sheaths. The Teflon™ sheaths were machined to be compatible with a Tacussel EDI rotator and CONTROVIT controller.

Electrodes were mechanically polished prior to each experiment with successively finer grades of SiC paper down to 600 grit. This was followed by polishing on microcloth (Buehler) with 0.3 micron alumina on a polishing wheel and a final hand polish with 0.05 micron alumina on microcloth.

Additive solubilities were determined in solutions containing 7% by weight ZnO and 2% by weight of the additive in 45% KOH. The solubility of ZnO is approximately 5.5% by weight under these conditions; hence some solid ZnO was always present. The solutions containing additives were stirred at room temperature for a minimum of 72 hours prior to analysis by atomic absorption spectrometry and electrochemical testing.

Zinc oxide powder (USP-20) was supplied by New Jersey Zinc Co. All other chemicals were of reagent grade and supplied by Fisher Scientific. Water was purified in an ion exchange cartridge system with a resulting resistivity of at least 13 megohm-cm.

The electrochemical instrumentation consisted of an EG&G PAR Model 173 potentiostat/galvanostat equipped with a Model 179 digital coulometer and a Model 175 universal programmer. Data were recorded on a Bascom Turner Model 8120-A digital storage X-Y plotter and stored on magnetic disks.

In the chronopotentiometric studies, the current was pulsed from zero current to preselected current densities of 10 mA cm^{-2} or less employing a 5 millisecond pulse. The potential response was recorded on a Tektronix Model 7623A oscilloscope equipped with a 7A22 Differential Amplifier and 7B53A Dual Time Base. A pulse was used, rather than a current step, in order to return the electrode to equilibrium after each measurement. This procedure avoids excessive changes in electrode surface area and provides reproducible results.

Chronocoulometry data were obtained by recording the output of a PAR Model 179 digital coulometer as a function of time following a potential step from the rest potential to a potential in the zincate reduction region. After 5 seconds, the electrode was returned to its rest potential. The electrode was potential cycled between experiments to provide a reproducible electrode surface. The charge (Q) vs. time data were recorded on magnetic disk using a Bascom Turner Model 8120-A recorder. For analysis via the algorithm, data were transferred to a Hewlett Packard Model 9825A desktop computer via an RS 232 interface. A computer program utilizing the algorithm was used to produce the semi-derivative data.

Fabrication of the pasted electrodes involves pressing zinc oxide powder containing additives and binder material such as polyvinyl alcohol or carboxymethylcellulose (1 w/w %) onto a silver screen. The pressed electrode is enclosed in a paper envelope (ALDEX 74 or 213, Aldin Paper Co.) to maintain physical stability during subsequent steps in the fabrication process. Electrodes constructed in this laboratory are 3 cm x 3 cm x 0.1 cm and are pressed to a final density of 2.25 g/cm^3. After pressing, the electrode is "formed" as the zinc oxide is slowly reduced electrochemically to metallic zinc in 5% KOH. Problems with poor physical stability due to swelling of the paper envelope and redistribution of the zinc oxide powder were encountered in this step when the electrodes were mounted vertically in the forming cell. These problems were eliminated by using a horizontal electrode configuration and applying a constant pressure on the face of the electrode during formation. The pressure is maintained by several layers of PELLON separator material (Freudenberg Co.) tightly sandwiched between the zinc electrode and the nickel screen counter electrode. After formation, the zinc deposits were compact, adherent, and showed excellent physical stability.

4. RESULTS AND DISCUSSION

4.1 CYCLIC VOLTAMMETRY AT A SILVER DISK ELECTRODE

Silver screens are commonly employed as current collectors for the zinc electrode in military Ag-Zn cells, hence we studied the deposition of zinc and various additives at a silver electrode. The concentration of additives in the supernatant liquids was determined by atomic absorption spectrometry after a minimum equilibration period of 72 hours (Table I). The excess of ZnO solid in each sample was deliberate and served to simulate open circuit conditions for a discharged pasted electrode. The solubilities measured in this manner are in excess of the amount of additive that may be absorbed on the ZnO powder. The most soluble additives are PbO, SnO, and WO_3, with concentrations approaching the value for complete dissolution at the 2% additive level. Bi_2O_3, $In(OH)_3$, and HgO show solubilities in the intermediate range from 45 to 75 ppm. The least soluble additives in 45% KOH are CdO, Ti_2O_3, Fe_2O_3, TiO_2, V_2O_4, and SnO_2. The solubility of an additive may indicate whether the additive produces a substrate effect (insoluble additives) or interactive effects during zinc electrodeposition (soluble additives). These interactive effects are discussed in a later section.

The general current-voltage (CV) behavior of a silver disk electrode in 45% KOH is shown in Figure 1. A broad double layer region extends from 0.0V to approximately -1.20V. Oxidation of silver occurs at potentials

more positive than 0.15V and reduction of silver oxide is evident as a large cathodic peak at ~0.10V. The CV response with zincate ion present is shown in Figure 2. Reduction of zincate ion to zinc occurs at potentials negative to -1.36V. A small shoulder is evident prior to bulk zincate reduction. Zinc is known to form alloys with silver (12) and to underpotentially deposit on Ag (4). Either of these processes can give rise to the shoulder on the reduction wave. Stripping of bulk zinc is evident by the large stripping peak present at -1.37V. Stripping of either the alloy phase or the underpotential deposit is believed to give rise to the additional oxidation peaks observed at -1.15V and -0.25V. Changes in the CV response with various additives present in the electrolyte are discussed in the following section. Samples of the supernatant solution were used in all cases.

PbO: This, along with SnO, is the most soluble of all the additives studied (700 ppm). It produces substantial changes in the current voltage response as seen in Figure 3. The reactions and standard reduction potentials for PbO_2 and $HPbO_2^-$ are:

$$PbO_2 + H_2O + 2e = PbO + 2OH^- \qquad E^\circ = 0.25 \text{ vs. N.H.E.}$$

$$HPbO_2^- + H_2O + 2e = Pb + 3OH^- \qquad E^\circ = -0.54 \text{ vs. N.H.E.}$$

These data suggest that metallic Pb is present on the electrode prior to the initial stages of zinc deposition. The presence of lead significantly reduces the rates of zincate reduction and zinc oxidation. The multiple oxidation peaks in the region from -0.40V to -0.80 volts correspond to the oxidation of both bulk and underpotentially deposited (UPD) Pb on silver. The PbO additive also influences the silver oxide region.

CdO: The additive has a low solubility (20 ppm) and there is no current response that is directly attributable to the cadmium oxide (Figure 4). The slight changes in the zinc alloy/UPD response suggests that there may be an interaction of cadmium in the early zinc layers. No obvious differences were observed in bulk zinc plating and stripping. As one might anticipate, the combination of PbO and CdO additives yields a response similar to that of PbO alone (Figure 5).

Bi_2O_3: Significant changes in the CV response of the silver disk electrode were noted with Bi_2O_3 present despite its fairly low solubility (60 ppm). These changes are illustrated in Figure 6. A major reduction in the rate of zinc deposition is evidenced by the increased slope of the reduction wave and the reduced stripping peak. The alloy or UPD zinc responses are not present and several new peaks are evident. The standard reduction potential for the reaction:

$$Bi_2O_3 + 3H_2O + 6e = 2Bi + 6OH^-$$

is -0.46V; hence, the oxidation peak at -0.35V and the reduction peak at -0.5V are believed to result from the redox behavior of a film of Bi_2O_3 on the electrode surface.

In_2O_3: The additive is soluble to the extent of 45 ppm and the principal effect of the additive appears to be the suppression of the alloy/UPD peaks (Figure 7). The small oxidation peak at -1.10V is believed to be due to the oxidation of indium to In_2O_3 with a reversible potential of -1.10V (4).

Tl_2O_3: This additive is essentially insoluble in 45% KOH and the current-voltage curve shown in Figure 8 is virtually identical to the additive-free case shown in Figure 2.

HgO: Significant changes in the current-voltage response of the Ag electrode were noted (Figure 9). A sharp peak is evident close to bulk zincate reduction. The zinc alloy (or UPD) peak at -1.20V is absent. A broad oxidation region is evident at 0.10V and an additional reduction peak is observed at 0.0V. No significant changes in the zinc oxidation region are observed. The concentration of the additive corresponds to ~70 ppm.

SnO_2: No changes in the CV response is observed in the presence of SnO_2 due to its low solubility (Figure 10).

SnO: The small stripping peak at -1.05V may be due to alloy formation (Figure 11). A second small stripping peak at -0.730V is also evident. At high scan rates (>500 mV/s), a broad oxidation region is observed from -0.30V to the onset of Ag oxidation. A long, broad reducton current follows AgO reduction, suggesting a UPD process over several hundred millivolts. The solubility of SnO in 45% KOH equals that of PbO (Table I).

CeO_2, V_2O_4, TiO_2, WO_3 and Fe_2O_3: No significant changes are observed in the CV response due to these additives (Figures 12-16). Most have low solubilities, except WO_3 (Table I).

Cyclic voltammetry studies clearly indicate that certain additives (Pb, Bi) influence not only the cathodic (deposition) but also the anodic (dissolution) behavior of Zn in 45% KOH. Although this is to be expected, little attention has been paid to the effect of additives on the dissolution process. This aspect clearly warrants further study.

The effect of additives on the CV profile of Zn deposition/dissolution cannot be easily correlated to the additive solubility in 45% KOH. Profound changes are observed in the presence of PbO, whose solubility is 700 ppm, but no substantial changes were seen in the presence of SnO, whose solubility is comparable to that of PbO. Reduction in the kinetics of bulk zinc plating and stripping and major shifts in zinc underpotential deposition are also seen in the presence of Bi_2O_3, whose solubility is only 60 ppm. Yet, In_2O_3 additive, whose solubility parallels that of Bi_2O_3, has no effect on zinc kinetics, and the only change observed in CV behavior is a suppresion of Zn UPD. Thus, solubility is not the overriding factor in the effect of additives on the kinetics of zinc deposition/dissolution. It appears that simple substrate effects can also be ruled out, since all four additives have reduction potentials more positive than Zn. These data suggest that an interactive effect (or lack thereof) during zinc electrodeposition/dissolution is responsible for the observed behavior.

4.2. CYCLIC VOLTAMMETRY AT A ZINC DISK ELECTRODE

In practical battery systems, zinc deposition occurs at a rapid rate and the influence of the substrate is exerted directly only for the first few zinc layers. This influence can be significant if it results in a change in the nucleation process or the kinetics of crystal growth (5, 6, 13). The more soluble additives can also interact with the zinc deposition process at later stages when the process is essentially the deposition of zinc onto a zinc substrate. The influence of some of the more soluble additives on zinc deposition at a pure zinc substrate was therefore examined by cyclic voltammetry.

The current-voltage response of a pure zinc disk electrode in 45% KOH containing 5.5% ZnO is shown in Figure 17A. Several sweeps are recorded at scan rates of 10, 20, 50, 100, 200, and 500 mV/s with the highest scan rate giving rise to the largest peak currents. There is very little current response in the passive region from +0.40V to approximately -1.00V. Breakdown of the passive film on the electrode gives rise to the sudden increase in current as the potential is made more negative than -1.00V (see also 1, 14). Dissolution of the zinc electrode occurs readily in the region from -1.00V to -1.36V. Bulk deposition of zinc occurs at potentials more negative than -1.36V and stripping of the zinc deposit is evident as the electrode potential is made more positve in the region from -1.40V to -1.00V. The Bi_2O_3 and HgO additives have little effect on the current-voltage response of the zinc electrode as shown in Figures 17B and C. In the presence of PbO, (Figure 17D), the current becomes noisy and spurious peaks are observed. The co-deposition of Pb occurs

in this potential region (-0.70V to -1.80V) and is probably responsible for the erratic current behavior.

It is possible to distinguish between reversible, irreversible, or quasi-reversible kinetic behavior by plotting the peak current for the reduction of zinc versus the square root of the potential scan rate (15). Reversible behavior (rapid kinetics) yields a linear plot and the peak potential is independent of scan rate. Irreversible kinetics also yields a linear plot of peak current versus square root of the scan rate but the peak potential shifts with scan rate. Intermediate or quasi-reversible kinetics do not yield linear plots of peak current versus square root of the scan rate. (Interpretation of the oxidation kinetics from cyclic voltammetry curves is difficult since the anodic peak depends on the amount of metal deposition in the previous cathodic sweep (16).)

The peak currents versus (scan rate)$^{1/2}$ for the data in Figure 17 are plotted in Figure 18 for the case with no additive and with HgO present, and in Figure 19 for the PbO and Bi_2O_3 additives. With no additives present (Figure 18), a linear response for the oxidation of zinc is observed and very little shift in the peak potential is evident. (All data were obtained with IR compensation using the procedure recommended by the potentiostat manufacturer.) The plot for the reduction process shows definite curvature and quasi-reversible kinetics. Intermediate kinetics are also observed for the reduction process in the presence of HgO, Bi_2O_3 and PbO additives.

The merit of scan rate studies during linear scan voltammetry experiments is that they provide a rapid ball-park estimate of the kinetics. If the current-voltage response suggests reversible or completely irreversible kinetics, it is often possible to extract kinetic parameters directly from the CV data. Unfortunately, for the case of quasi-reversible kinetics, the mathematical solutions are difficult because many of the simplifying assumptions used in the reversible or irreversible cases are not appropriate. Other techniques such as chronopotentiometry and chronocoulometry yield more tractable mathematics and were therefore chosen to determine the kinetic parameters for the zinc electrode reaction in the presence and absence of additives.

4.3. CYCLIC VOLTAMMETRY AT A PASTED ZnO ELECTRODE

Limited studies were conducted with pasted ZnO electrodes with and without additives. Current-potential profiles were recorded on "green" or unformed electrodes. On a fully formed electrode, the current is more than 30 times larger in the anodic region than for the unformed electrode and a peak is only observed if electrode passivation occurs. For this reason, cyclic voltammetry on fully formed electrodes yields limited information and it was not pursued further.

A typical current-voltage response for a pasted ZnO electrode with no additives is shown in Figure 20 for 5% KOH. A large reduction current due to ZnO reduction is seen in region A. Upon scan reversal, the metallic zinc formed in A is reoxidized to ZnO giving rise to peak B. A current peak is observed because of the limited amount of metallic zinc formed in region A. The broad shoulder in region C is the result of oxidation of an alloy formed between the silver current collector and zinc. Hendrikx et al. (12) have identified this peak as the ε-phase of $AgZn_3$ alloy. The oxidation and subsequent reduction of the silver current collector is evident in regions D and E respectively. The overall current-voltage curve is centered on the zero current line with very little slope, indicating a low resistance electrode. A high resistance in the electrode would generate an IR voltage drop which would tend to distort the current-voltage profile. The response of the pasted electrode is remarkably similar to the response for a solid silver electrode in the presence of zincate ions (Figure 2).

Addition of PbO influences the pasted electrode CV response. Data for a ZnO electrode containing 1% PbO additive are shown in Figure 21. Three additional peaks, F, G, and H, are evident in the CV response. Peak H corresponds to the reduction of PbO to Pb ($E^{\circ\prime}$ =0.73 V vs Hg/HgO). Peaks F and G are believed to arise from the oxidation of PbO to PbO_2 (peak F) and the reverse reaction (peak G). Cyclic voltammograms for a pure lead electrode in 45% KOH showed PbO oxidation at +0.500 V and PbO_2 reduction in a region from -0.400 V to -0.800 V, depending on the KOH concentration. The zinc oxide reduction current is shifted to more negative potentials in the presence of PbO and the peak associated with the formation of the $AgZn_3$ alloy is absent.

Similar data are obtained when lead additive is used in conjunction with CdO, except in the anodic region, where the Zn oxidation peak is conspicuously absent, while two additional peaks appear (Fig. 22). Peak A in Fig. 22 represents the reduction of PbO_2 to PbO; peak B is the reduction of PbO to Pb; wave C corresponds to the reduction of CdO to cadmium metal and peak E to its reoxidation; and finally, peak D corresponds to the oxidation of Pb to PbO. The silver oxide region is also strongly affected by the presence of PbO whereas CdO has little effect. The electrode response with only CdO present (2%) is shown in Fig. 23. As expected, peaks B and D are absent, while the wave in region C and the peak in region E are evident as they were in the previous case for both PbO and CdO present. Interestingly, an anodic peak due to zinc oxidation is again evident even though both the cathodic and anodic zinc reaction rates appear equally

suppressed. In the presence of CdO as a solution additive no reduction in the rate of zinc deposition/dissolution was observed at a Ag electrode (Figure 4).

It should be emphasized that work with pasted electrodes could be of little quantitative value since no two pasted electrodes are exactly the same. Precise measurements of surface area and electrode resistance are necessary for meaningful comparison. Also, no kinetic data on zinc deposition/dissolution could be derived from studies with pasted electrodes. Thus, the information obtained by cyclic voltammetry should be viewed for trends only. However, the ability to directly monitor the redox behavior of additives in the paste by cyclic voltammetry suggests that chronopotentiometry during the forming process may be of use in determining the oxidation state and percent conversion of the additives (17).

4.4. CHRONOPOTENTIOMETRIC STUDIES OF ZINCATE REDUCTION

The technique of chronopotentiometry involves monitoring the voltage response of an electrode subjected to a current step or pulse. In the absence of mass transfer effects, the relationship of overpotential (η) to the current is represented by the Butler-Volmer equation:

$$i = i_o[\exp(-\alpha n f \eta) - \exp[(1-\alpha) n f \eta] \qquad (1)$$

where i_o is the exchange current density, α is the transfer coefficient, n is the number of electrons transferred in the rate determining step and f=F/RT. This equation is valid provided i is small compared to the limiting current and the measurement is completed in a sufficiently short time that mass transfer effects are negligible. Provided these conditions are met, chronopotentiometry allows one to obtain values of αn and i_o, important kinetic parameters.

The cyclic voltammetry results indicate quasi-reversible kinetics for the zinc electrode (Section 4.1). For this case, the opposing charge transfer reaction must be considered at low overpotentials. Using the method of Allen and Hickling (18), equation (1) can be rewritten as:

$$i = i_o \exp(-\alpha n f \eta)[1-\exp(n f \eta)] \qquad (2)$$

or, in logarithmic form as:

$$\ln \frac{i}{1-\exp(n f \eta)} = \ln i_o - \alpha n f \eta \qquad (3)$$

Therefore, a plot of the lefthand side of equation (3) versus overpotential should yield a linear plot of slope $-\alpha n f$ and intercept of $\ln i_o$.

Results for a zinc electrode in 45% KOH with no additives present are shown in Figure 24 for zincate concentrations of 5.5% and 1.1%. Two linear portions of different slopes intersecting at $\eta=0$ are observed. Values of the exchange current density calculated from the intersection are 2.1 and 2.2 mA cm^{-2} for 5.5% and 1.1% ZnO, respectively. Slopes of the linear cathodic and anodic portions of the curve yield the indicated values of the cathodic and anodic transfer coefficients (for n=2); in both cases the sum of $\alpha_c + \alpha_a$ is close to unity.

A series of seven replicate experiments provided the results shown in Table II. Good agreement is observed with an average value for i_o of 2.2 mA cm^{-2}.

4.5. CHRONOCOULOMETRIC STUDIES OF ZINCATE REDUCTION

A useful technique for evaluating the electrochemical response of a system is to integrate the current, obtaining the charge Q as a function of time. This technique, known as chronocoulometry (19), offers several experimental advantages for kinetic studies. Since the response increases with time, the later parts of the transient offer good signal-to-noise ratios. Since the later transient response is more experimentally accessible, chronocoulometry requires less sophisticated equipment. Moreover, because the evaluation of rate parameters is made by extrapolation from a later time domain, it is more easily applied to fast, or moderately fast reactions. The chronocoulometric record is less subject to noise since the current is integrated. A comprehensive discussion of chronocoulometry and its application to heterogeneous kinetics may be found in Ref. 15.

Experimentally, the charge passed at the electrode is measured as a function of time following a potential step from a region where there is no electrode reaction to an active region where the reaction occurs at a kinetic (low η) or mass transport (high η) limited rate. For quasi-reversible kinetics, the electrode charge as a function of time, Q (t), is given by,

$$Q(t) = \frac{nFAk_f C_o^b}{H^2} \left[\exp(H^2 t)\operatorname{erfc}(H\sqrt{t}) + \frac{2H\sqrt{t}}{\sqrt{\pi}} - 1\right] \qquad (4)$$

where

$$H = (k_f/\sqrt{D_o}) + (k_b/\sqrt{D_R}) \qquad (5)$$

and the other terms have their usual electrochemical significance. For $H\sqrt{t} > 5$, the complement of the error function approaches zero, and a

plot of Q vs $\sqrt{t}$ should yield a linear portion of slope:

$$\frac{dQ}{d\sqrt{t}} = \frac{2nFAk_f C_o^b}{H\sqrt{\pi}} \tag{6}$$

and the intercept of the linear portion on the Q=0 axis is given by:

$$\sqrt{t_i} = \frac{\sqrt{\pi}}{2H} \tag{7}$$

Experimentally, H is determined from the intercept, $\sqrt{t_i}$, and k_f is calculated from the experimentally determined slope via Eq. 6. Despite the advantages of chronocoulometry, this technique has not been widely used because of the complex nonlinear charge-time relationship when the response is either partially or fully governed by charge transfer kinetics. Since the linearization approximation for Q vs $\sqrt{t}$ is valid only for $H\sqrt{t} > 5$, one is not able to use the entire data set and this constraint may present experimental difficulties, particularly for low values of H.

Oldham(20) has recently presented an alternative approach for the interpretation of chronocoulometric data that allows linearization of the entire data set without prior knowledge of the kinetic parameters. This approach is based on convolution of the charge-time data via a semidifferentiation algorithm. The algorithm provides a set of semidervative data, m(t), which can be combined with the charge data to yield the simple equation:

$$\frac{m(t)}{\sqrt{t}} = \frac{2I_o}{\sqrt{\pi}} - \frac{Hq(t)}{\sqrt{t}} \tag{8}$$

where I_o is the initial current, which is not generally experimentally accessible. (We have denoted this as I_o to avoid confusion with i_o, the conventional designation for exchange current.) A plot of $m/\sqrt{t}$ vs $q/\sqrt{t}$ should be linear with a slope of -H and an intercept of $2I_o/\sqrt{\pi}$. The rate constant can be calculated from the equation:

$$I_o = nFAC_o^b k_f \qquad (9)$$

Chronocoulometric data were collected for zincate reduction in both the presence and absence of additives. Kinetic parameters were evaluated from both Q vs $\sqrt{t}$ data and $m/\sqrt{t}$ vs $q/\sqrt{t}$ data.

A typical chronocoulometric Q vs $\sqrt{t}$ data set for the reduction of zincate ion at a Ag electrode is shown in Figure 25 for an overpotential of -120 mV. Extrapolating the linear portion of the data, a value for H and $\sqrt{t_i}$ can be determined and a value of $k_f = 3.0 \times 10^{-3}$ cm s^{-1} is calculated.

Values of the potential dependent term H were calculated from Q vs $\sqrt{t}$ data at various overpotentials and ranged from approximately 0.4 $s^{-1/2}$ at low overpotentials to 2.5 $s^{-1/2}$ at high overpotentials. Since the approximation used for calculating k_f from Q vs $\sqrt{t}$ is valid only for $H\sqrt{t} > 5$, the time required for a valid approximation increases from 4 to 150 seconds as the overpotential is decreased. Figure 26 shows Q vs $\sqrt{t}$ at $\eta = -40$mV. At this potential, the linear portion of the plot includes only a fraction of the data set and does not allow an accurate determination of $\sqrt{t_i}$ or k_f.

While this problem could be solved by taking data for a longer time period, our experiments show that conditions of semi-infinite linear diffusion to a planar electrode can only be maintained for approximately 30 seconds when high zincate concentrations (1.2 M $Zn(OH)_4^{2-}$ in 11.6 M KOH) are used due to large changes in electrode morphology at longer times. Given the 30 second time constraint to maintain well-defined diffusion conditions, the use of approximations is prohibited on data obtained at overpotentials less than approximately 100mV.

Since charge transfer control predominates at low overpotentials where the classical approximation method fails, the use of Oldham's algorithm was explored as a means of analyzing chronocoulometric results. Since no approximations are required and the entire data set is utilized, kinetic parameters should be calculable even at low overpotentials.

A computer program was developed to convert Q vs $\sqrt{t}$ data to $m/\sqrt{t}$ vs $q/\sqrt{t}$ data. The accuracy of the algorithm program was tested by generating a sample set of charge versus time data calculated from Eq. 4 using values of H=1.00 and I_o=375 mA cm^{-2} (typical for zinc deposition at low to moderate overpotentials). The sampling interval was 0.1 seconds over an experimental duration of 5 seconds. A plot of the data generated by the algorithm is shown in Figure 27. The plot is linear throughout the entire range of data and yields values of 0.998 for H and 374.6 mA cm^{-2} for I_o.

The algorithm was applied to chronocoulometry data for zincate reduction in the absence of additives. Typical data for η=-40 mV and η=-120 mV

are shown on Figures 28 and 29. While there is some scatter in the data, the points give a good linear fit for the entire data set, as opposed to the Q vs $\sqrt{t}$ data, particularly for low η.

Values of I_o at various overpotentials were calculated from the intercept. The potential dependent rate constant, k_f, was calculated from Eq. 9. A value of k_o was then calculated from the relationship:

$$k_f = k_o \exp(-\alpha n f \eta) \qquad (10)$$

The value for $n\alpha$ is determined from a plot of log H vs potential (Figure 30) and log I_o vs potential (Figure 31). The slope of the linear portion of each plot at more negative potentials is equal to $-\alpha nf/RT$ and hence the Tafel slope and transfer coefficient can be determined. From these plots a Tafel slope of 142 mV was determined, giving a value for $n\alpha=0.42$.

The results obtained for zincate reduction at a Ag electrode are summarized in Table III. A value of $k_o=2.40\pm 0.22\times10^{-4}$ cm s^{-1} is obtained via the algorithm. At higher overpotentials, H approaches $k_f/\sqrt{D_o}$ as $k_b/\sqrt{D_o}$ approaches zero. From the slope of $m/\sqrt{t}$ vs $q/\sqrt{t}$, one calculates a diffusion coefficient $D_o=2.3\times10^{-6}$ cm^2 s^{-1} for zincate in 11.2M KOH, which agrees well with the published values of 1.52×10^{-6} cm^2 s^{-1} by McBreen(21) and 3.43×10^{-6} cm^2 s^{-1} by Dirkse(22).

The kinetic parameters determined by the algorithm for zincate reduction are in good agreement with published values. The Tafel slope of 142 mV compares well with the value of 113± 30mV reported by Bockris et al.(23)

for 0.5M zincate in 3M KOH. The ratio of $k_o/\sqrt{D_o}$ is reported by Payne and Bard(24) as 0.17 for Zn(II) reduction at mercury and our experiments yield a similiar value of 0.16 for Zn(II) reduction at silver.

Chronocoulometry experiments were also carried out in 1.2M $Zn(OH)_4^{2-}$ in the presence of additives. Since PbO is known to have a beneficial effect on commercial Zn electrodes, it was decided to concentrate our studies on this additive. Unfortunately, extraction of any kinetic information in the presence of additives was much less tractable. Attempts to use the semi-differentiation algorithm in the presence of PbO were unsuccessful. We believe this to be due to complications arising from the co-reduction of Pb(II) during zincate reduction. The situation is further complicated by the possible contribution of charge due to hydrogen evolution.

In an attempt to correct for the charge contribution due to lead additive, experiments were carried out in KOH, PbO in the absence of zincate (Figure 32). This chronocoulometric data set was subtracted from the data set for zincate reduction in the presence of lead. Once again, the resultant plots would not yield tractable kinetic parameters.

While it is not possible to make accurate quantitative statements about the presence of Pb(II) on the kinetics of zincate reduction, chronocoulometry shows that the presence of Pb(II) has a strong effect on zincate reduction at Ag. A comparison of Q vs t for zincate reduction in the absence and presence of Pb(II) shows that the rate of Zn(II) reduction is significantly lower in the presence of lead additive (Figure 33).

We believe this reduction in the rate of zinc deposition is due to the codeposition of lead. A rotating ring-disk electrode was employed to show that Pb(II) reduction was occurring concurrent with zincate reduction. The disk and ring current as a function of disk potential is shown in Figure 34. The ring is held at a constant potential of -1.00V, at which potential Pb(II) is reduced, but not zincate. Hence the ring current provides a monitor only of Pb ion flux. At potentials anodic of zincate reduction, the ring becomes shielded due to the reduction of Pb(II) at the disk. The ring electrode remains fully shielded throughout the cathodic potential sweep, suggesting that zinc and lead are co-deposited.

Mansfield and Gilman (25) have reported that zinc deposition on the basal plane of single crystal zinc is epitaxial in the absence of plumbate ion. However, when plumbate ions are present, a smooth film of metallic lead forms on the zinc crystal and the initiation and growth of the zinc deposit tends to be mainly at sites not covered by lead. We believe a similar process is responsible for the reduced rate of zincate reduction observed in our results. A lead film forms during the initial stages of deposition. The high solubility of PbO in the electrolyte provides a continuous plumbate reduction process and hence the lead film is continuously renewed and the interaction with adjacent zinc layers is maintained.

It is important to distinguish this dynamic atom-layer by atom-layer interaction from a simple substrate effect. In the absence of significant alloy formation, a substrate effect should be limited to only those zinc

layers in direct contact with the substrate. The rapid formation of subsequent zinc layers obscures the substrate in milliseconds and there is no mechanism by which the substrate interaction can be renewed except by complete stripping of the zinc deposit.

Figure 35 shows the chronocoulometric response for zincate reduction at Pb, Zn and Ag. The substrate is seen to have little affect on the Q vs t behavior and the kinetics are essentially those of zincate reduction at zinc. (The slight variations are due to different roughness factors for the electrodes.) A comparison of Figures 33 and 35 clearly indicates that solubility and the ability to codeposit with zinc are important properties for the PbO additive.

5. CONCLUSIONS

Analysis of our results, obtained by several experimental techniques, points to a significant reduction in the zinc deposition rate in 45% KOH in the presence of the solution additive, PbO. The solubility of PbO in this medium is relatively high, being among the highest in the series of additives studied. The presence of plumbate ions modifies zinc deposition kinetics in a virtually identical manner for zinc and silver substrates. There is also no observable substrate effect in the absence of plumbate ions and even with a lead substrate the kinetics are indistinguishable from those with zinc or silver substrates. These results suggest that co-deposition of lead, leading to a dynamic atom-layer by atom-layer interaction rather than a simple substrate effect, is responsible for the observed reduction in the zinc deposition rate. The reduced rate of zinc deposition should lead to a more uniform deposit, which in turn should lead to a reduced zinc shape change upon cycling, as observed in commercial practice. While further work is in order (especially on the dissolution process of zinc, which is also affected by lead) our results point to the possibility of employing electrolyte additives, as opposed to additives to the ZnO paste, in practical cells.

Successful employment in our work of Oldham's algorithm for the analysis of chronocoulometric data (in pure zincate solutions) indicates that this technique could be extended to studies of systems other than zincate.

6. ACKNOWLEDGEMENTS

This work was supported in part by the Office of Naval Research. Dr. T. Palamisamy's contribution in preparing the original proposal (with D. C.) is greatly acknowledged. The authors are also indebted to Dr. P. Gifford for his help in the interpretation of chronopotentiometic and chronocoulometric results, and revision of the final manuscript.

7. REFERENCES

1. J. McBreen and E. J. Cairns, in "Advances in Electrochemistry and Electrochemical Engineering," Vol. 11, H. Gerischer and C. W. Tobias, Editors, p. 273, John Wiley and Sons, New York (1978).

2. O. Wagner and A. Himy, Proc. 27th Power Source Symposium, 1976, p. 135.

3. A. Himy and O. Wagner, U. S. Patent 4,084,047 (1978).

4. J. McBreen and E. Gannon, Electrochim. Acta, 26 (1981) 1439.

5. M. G. Chu, J. McBreen and G. Adzic, J. Electrochem. Soc., 128 (1981) 2281.

6. J. McBreen, M. G. Chu and G. Adzic, ibid., 128 (1981) 2287.

7. S. Fletcher, R. Deutscher, C. Harvey, R. Woods, E. J. Fraser, T. Lwin, G. Nelson and D. Gates, ILZRO Project No. ZE-295, Semi-Annual Progress Report No. 2, November 1981.

8. J. McBreen, J. Electrochem Soc., 119 (1972) 1620.

9. R. L. Deutschez, S. Fletcher and J. Galea, J. Power Sources, 11 (1984), 7.

10. A. Himy and R. Karcher, The Electrochem. Soc. Meeting, Hollywood, FL, October 1980, Ext. Abs. No. 90.

11. R. Thacker, J. Chem. Ed. 45 (1980) 180.

12. J. Hendrikx, W. Visscher, and E. Barendrecht, Electrochim. Acta., 28 (1983) 743.

13. A. R. Despic and M. G. Pavlovic, ibid, 27 (1982) 1539.

14. M. H. Hull, J. E. Ellison and J. E. Toni, J. Electrochem. Soc., 117 (1970) 192.

15. A. J. Bard and L. R. Faulkner, Electrochemical Methods, Wiley, New York, 1980.

16. M. Elam, E. Peled and E. Gileadi, J. Electrochem. Soc., 130 (1983) 585.

17. J. McBreen, E. Grannon and M. G. Chu, The Electrochem. Soc. Meeting, Hollywood, FL, October 1980, Ext. Abs. No. 91.

18. P. A. Allen and A. Hickling, Trans. Faraday Soc., 53 (1950) 337.

19. F.C. Anson, Anal. Chem., 38 (1966) 54.

20. K.B. Oldham, J. Electroanal. Chem., 145 (1983) 9.

21. J. McBreen, Report No. N68-15716, Contract No. NAS 5-10231, Yardney Electric Corp., New York, June, 1967.

22. T.P. Dirkse, Technical Report No. AFAPL-TR-72-87, Contract No. S 33615-70-C-1022, Project 3145, Calvin College, Grand Rapids, MI., December, 1972.

23. J.O'M Bockris, Z. Nagy and A. Damjanovic, J. Electrochem. Soc., 119 (1972) 1665.

24. D.A. Payne and A.J. Bard, J. Electrochem. Soc., 119 (1972) 1665.

25. F. Mansfeld and S. Gilman, J. Electrochem. Soc., 117 (1970) 588.

8. LEGEND TO FIGURES

FIG. 1

Cyclic voltammogram of stationary silver electrode in pure 45% KOH. Electrode area: 0.0324 cm^2. Sweep rate: 50 mV s^{-1}.

FIG. 2

Cyclic voltammogram of stationary silver electrode in 45% KOH containing 5.5% ZnO. Electrode area: 0.0324 cm^2. Sweep rate: 50 mV s^{-1}.

FIG. 3

Cyclic voltammogram of stationary silver electrode in 45% KOH containing 5.5% ZnO and 5 x 10^{-3} M PbO (nominal concentration). Electrode area: 0.0324 cm^2. Sweep rate: 50 mV s^{-1}.

FIG. 4

Cyclic voltammogram of stationary silver electrode in 45% KOH containing 5.5% ZnO and 5 x 10^{-3} M CdO (nominal concentration). Electrode area: 0.0324 cm^2. Sweep rate: 50 mV s^{-1}.

FIG. 5

Cyclic voltammogram of stationary silver electrode in 45% KOH containing 5.5% ZnO, 5 x 10^{-3} M PbO and 1 x 10^{-2} M CdO (nominal concentration). Electrode area: 0.0324 cm^2. Sweep rate: 50 mV s^{-1}.

FIG. 6

Cyclic voltammogram of stationary silver electrode in 45% KOH containing 5.5% ZnO and 5 x 10^{-3} M Bi_2O_3 (nominal concentrations). Electrode area: 0.0324 cm^2. Sweep rate: 50 mV s^{-1}.

FIG. 7

Cyclic voltammogram of stationary silver electrode in 45% KOH containing 5.5% ZnO and 5 x 10^{-3} M In_2O_3 (nominal concentration). Electrode area: 0.0324 cm^2. Sweep rate 50 mV s^{-1}.

FIG. 8

Cyclic voltammogram of stationary silver electrode in 45% KOH containing 5.5% ZnO and 5 x 10^{-3} M Tl_2O_3 (nominal concentration). Electrode area: 0.0324 cm^2. Sweep rate: 50 mV s^{-1}.

FIG. 9

Cyclic voltammogram of stationary silver electrode in 45% KOH containing 5.5% ZnO and 5 x 10^{-3} M HgO (nominal concentration). Electrode area: 0.0324 cm^2. Sweep rate: 50 mV s^{-1}.

FIG. 10

Cyclic voltammogram of stationary silver electrode in 45% KOH containing 5.5% ZnO and 5 x 10^{-3} M SnO_2 (nominal concentration). Electrode area: 0.0324 cm^2. Sweep rate: 50 mV s^{-1}.

FIG. 11

Cyclic voltammogram of stationary silver electrode in 45% KOH containing 5.5% ZnO and 5 x 10^{-3} M SnO (nominal concentration). Electrode area: 0.0324 cm^2. Sweep rate: 50 mV s^{-1}.

FIG. 12

Cyclic voltammogram of stationary silver electrode in 45% KOH containing 5.5% ZnO and 5 x 10^{-3}M CeO_2 (nominal concentration). Electrode area: 0.0324 cm^2. Sweep rate: 50 mV s^{-1}.

FIG. 13

Cyclic voltammogram of stationary silver electrode in 45% KOH containing 5.5% ZnO and 5 x 10^{-3} M V_2O_4 (nominal concentration). Electrode area: 0.0324 cm^2. Sweep rate: 50 mV s^{-1}.

FIG. 14

Cyclic voltammogram of stationary silver electrode in 45% KOH containing 5.5% ZnO and 5 x 10^{-3} M TiO_2 (nominal concentration). Electrode area: 0.0324 cm^2. Sweep rate: 50 mV s^{-1}.

FIG. 15

Cyclic voltammogram of stationary silver electrode in 45% KOH containing 5.5% ZnO and 5 x 10-3 M WO3 (nominal concentration). Electrode area: 0.0324 cm2. Sweep rate: 50 mV s-1.

FIG. 16

Cyclic voltammogram of stationary silver electrode in 45% KOH containing 5.5% ZnO and 5 x 10^{-3} M Fe_2O_3 (nominal concentration). Electrode area: 0.0324 cm^2. Sweep rate: 50 mV s^{-1}.

FIG. 17

Cyclic voltammogram of stationary zinc electrode in 45% KOH w/wo additives. Electrode area: 0.0324 cm^2. Sweep rates: 10, 20, 50, 100, 200, and 500 mV s^{-1}.

a. No additives present

b. $5x10^{-3}$ M Bi_2O_3 present (nominal concentration)

c. $5x10^{-3}$ M HgO present (nominal concentration)

d. $5x10^{-3}$ M PbO present (nominal concentration)

FIG. 18

Plot of peak current vs. square root of scan rate for zinc oxidation/reduction, as recorded in Figure 17.

a. No additives present

b. HgO present

FIG. 19

Plot of peak current vs. square root of scan rate for zinc oxidation/reduction, as recorded in Figure 17.

a. PbO present

b. Bi_2O_3 present

FIG. 20

Cyclic voltammogram of pasted ZnO electrode in 5% KOH. No additives present. Scan rate 1 mV s^{-1}.

FIG. 21

Cyclic voltammogram of pasted ZnO electrode in 5% KOH with with 1% PbO present. Scan rate 1 mV s-1.

FIG. 22

Cyclic voltammogram of pasted ZnO electrode in 5% KOH with 2% total PbO and CdO present (PbO/CdO ratio 1:2). Scan rate 1 mV s^{-1}.

FIG. 23

Cyclic voltammogram of pasted ZnO electrode in 5% KOH, with 2% CdO present. Scan rate: 1 mV s^{-1}.

FIG. 24

Chronopotentiometric data for stationary zinc electrode in 45% KOH containing ZnO. Electrode area: 0.0324 cm^2.

a. 5.5% ZnO present

b. 1.1% ZnO present

FIG. 25

Chronocoulometric data for stationary silver electrode in 45% KOH containing 5.5% ZnO. η = -120 mV.

FIG. 26

Chronocoulometric data for stationary silver electrode in 45% KOH containing 5.5% ZnO. η = -40 mV.

FIG. 27

Plot of data generated by the algorithm for a sample set of charge vs. time data.

FIG. 28

Chronocoulometric algorithm data for the reduction of zincate in 45% KOH in the absence of additives. η = -40 mV.

FIG. 29

Same as Figure 26, for η = -120 mV.

FIG. 30

Plot of log H (determined by algorithm) vs. potential for silver electrode in 45% KOH containing 5.5% ZnO.

FIG. 31

Plot of log I_o values (determined by algorithm) vs. potential for silver electrode in 45% KOH containing 5.5% ZnO.

FIG. 32

Chronocoulometric data for lead deposition at silver electrode in 45% KOH in the absence of ZnO.

FIG. 33

Chronocoulometric data for zincate reduction at silver electrode (45% KOH) w/wo PbO additive. Electrode potential 100mV negative to open circuit potential.

FIG. 34

Rotating ring-disk current vs. disk potential for zinc deposition in the presence of lead.

FIG. 35

Chronocoulometric data for zincate reduction at Pb, Zn and Ag electrodes. Electrode potential 100 mV negative to open circuit potential.

TABLE I. ROOM TEMPERATURE SOLUBILITIES OF VARIOUS ADDITIVES

IN 45% KOH IN THE PRESENCE OF ZnO

ADDITIVE	% ZINC	ADDITIVE CONCENTRATION* (PPM)
PbO	5.55	700 Pb
CdO	5.21	20 Cd
Bi_2O_3	5.22	57 Bi
$In(OH)_3$	5.56	45 In
Tl_2O_3	5.56	< 1 Tl
PbO + CdO	5.45	720 Pb + 14 Cd
Fe_2O_3	5.35	10 Fe
WO_3	6.84	546 W
TiO_2	5.32	< 1 Ti
V_2O_4	6.73	12 V
SnO	5.63	715 Sn
HgO	6.10	72 Hg
CeO_2	5.46	< 100 Ce
SnO_2	5.51	< 2 Sn

*Determined by atomic absorption spectrometry of the supernatant solution

TABLE II. KINETIC PARAMETERS FOR ZINC REDUCTION/OXIDATION

45% KOH AND 5.5% ZnO

Exp. #	i_o(mA cm^{-2})	$\alpha_c + \alpha_a$
1	2.1	1.05
2	3.4	1.09
3	2.1	1.05
4	2.2	1.07
5	1.6	1.18
6	1.8	1.09
7	2.0	1.00

TABLE III. KINETIC PARAMETERS FOR ZINCATE REDUCTION

CALCULATED FROM $m/\sqrt{t}$ vs. $q/\sqrt{t}$ DATA

E(volts)	η(mV)	I_o(mA cm^{-2})	H($s^{-1/2}$)	k_f(cm s^{-1})	k_o(cm s^{-1})
-1.425	-60	119.3	+0.384	5.15×10^{-4}	1.95×10^{-4}
-1.445	-80	205.3	+0.567	8.87×10^{-4}	2.41×10^{-4}
-1.465	-100	300.7	+0.768	1.30×10^{-3}	2.54×10^{-4}
-1.485	-120	428.3	+1.126	1.85×10^{-3}	2.60×10^{-4}
-1.505	-140	594.8	+1.626	2.57×10^{-3}	2.61×10^{-4}
-1.525	-160	790.0	+2.234	3.41×10^{-3}	2.49×10^{-4}
-1.545	-180	975.2	+2.796	4.21×10^{-3}	2.22×10^{-4}

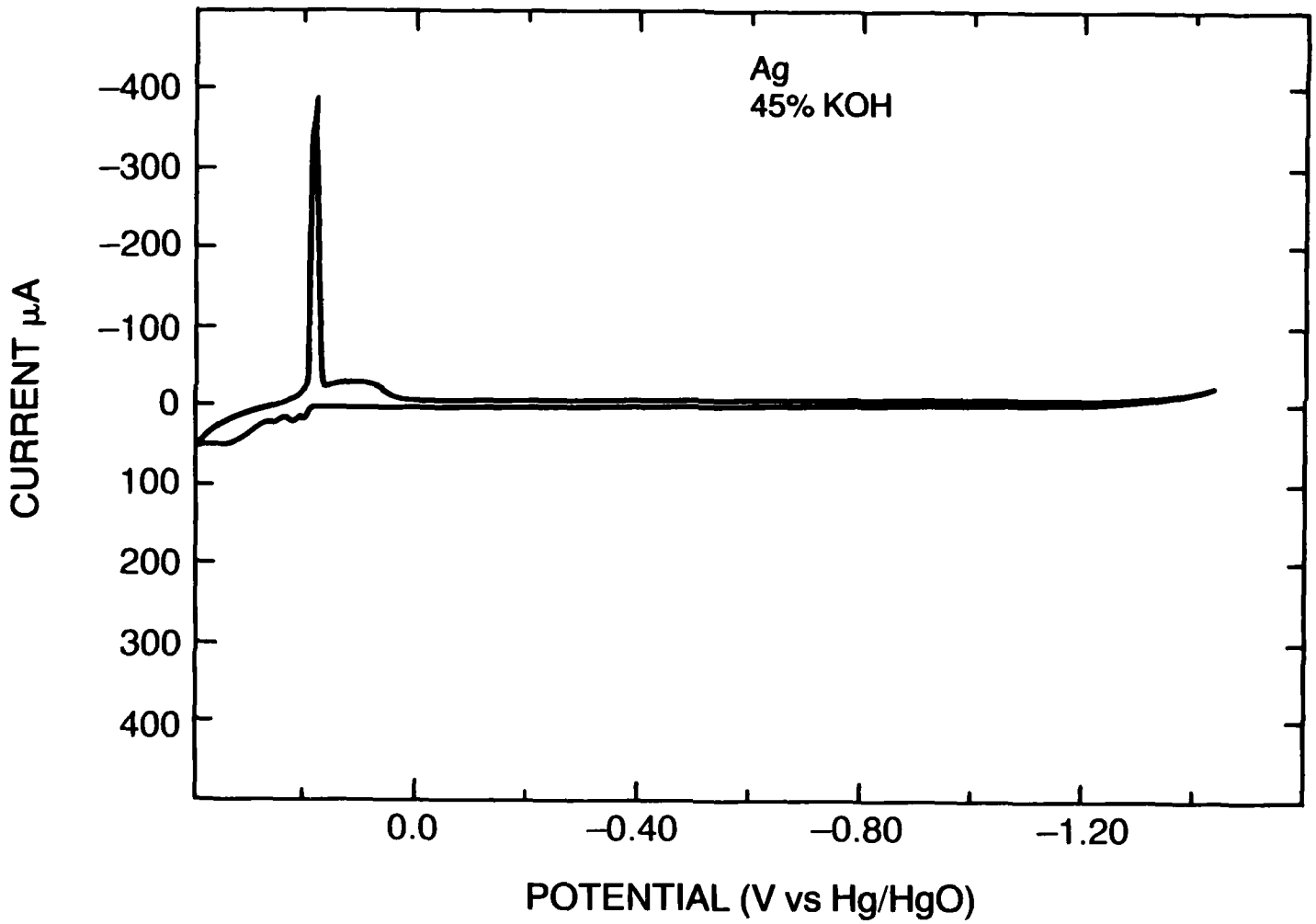
Ag
45% KOH
CURRENT μA
−400
−300
−200
−100
0
100
200
300
400
0.0
−0.40
−0.80
−1.20
POTENTIAL (V vs Hg/HgO)

Figure 1

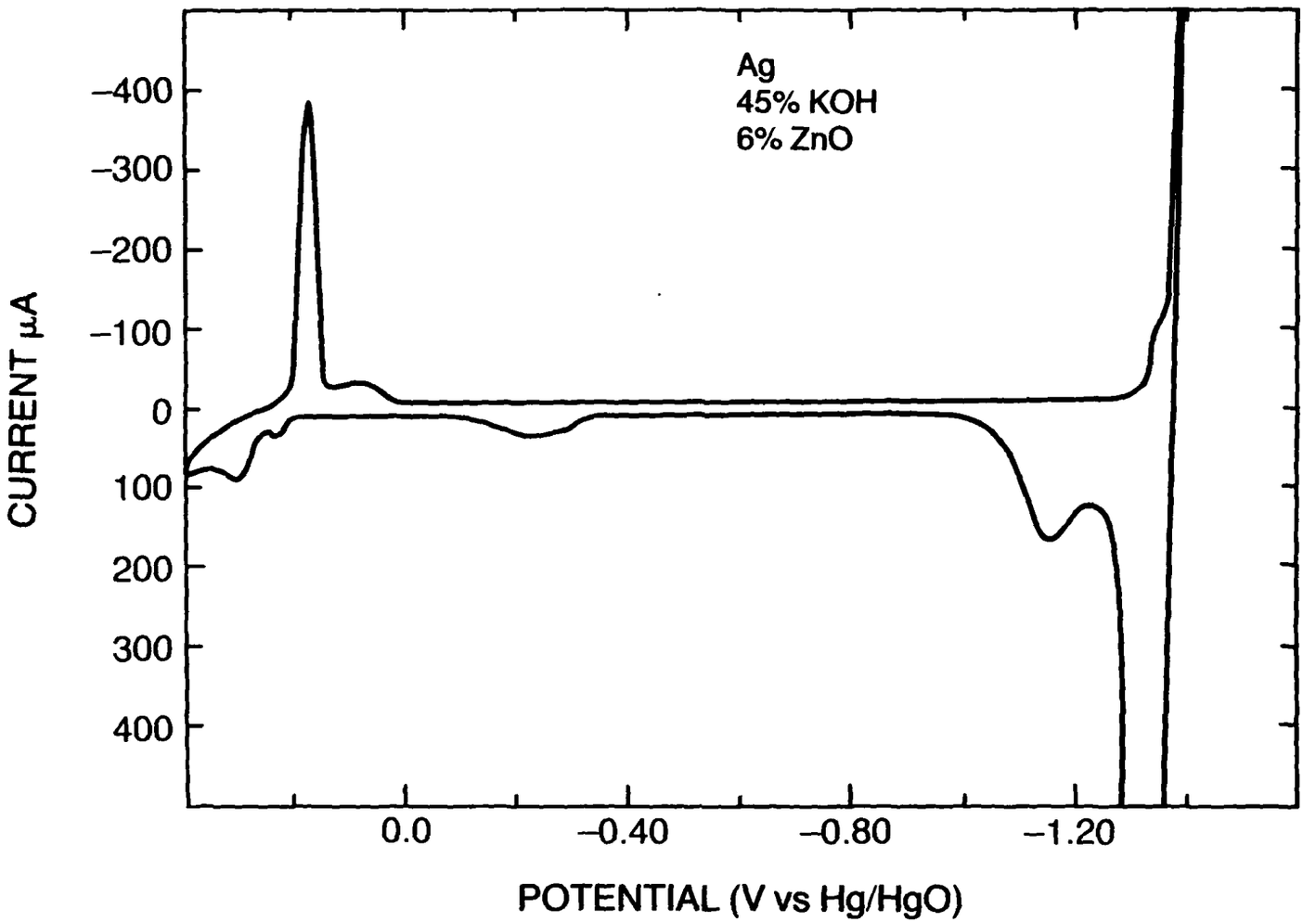
Ag
45% KOH
6% ZnO
CURRENT μA
−400
−300
−200
−100
0
100
200
300
400
0.0
−0.40
−0.80
−1.20
POTENTIAL (V vs Hg/HgO)

Figure 2

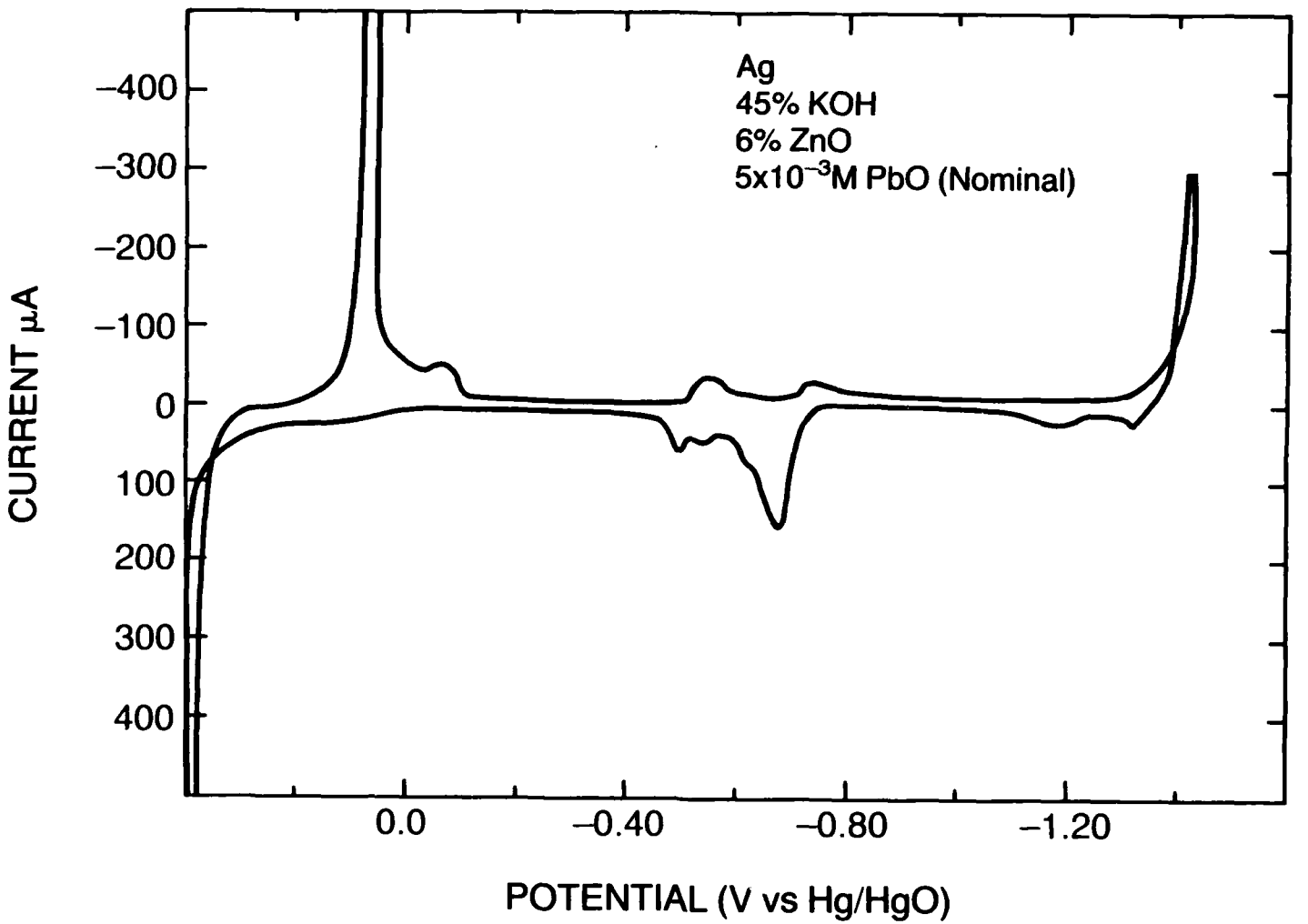
Ag
45% KOH
6% ZnO
5x10⁻³M PbO (Nominal)
CURRENT µA
−400
−300
−200
−100
0
100
200
300
400
0.0
−0.40
−0.80
−1.20
POTENTIAL (V vs Hg/HgO)

Figure 3

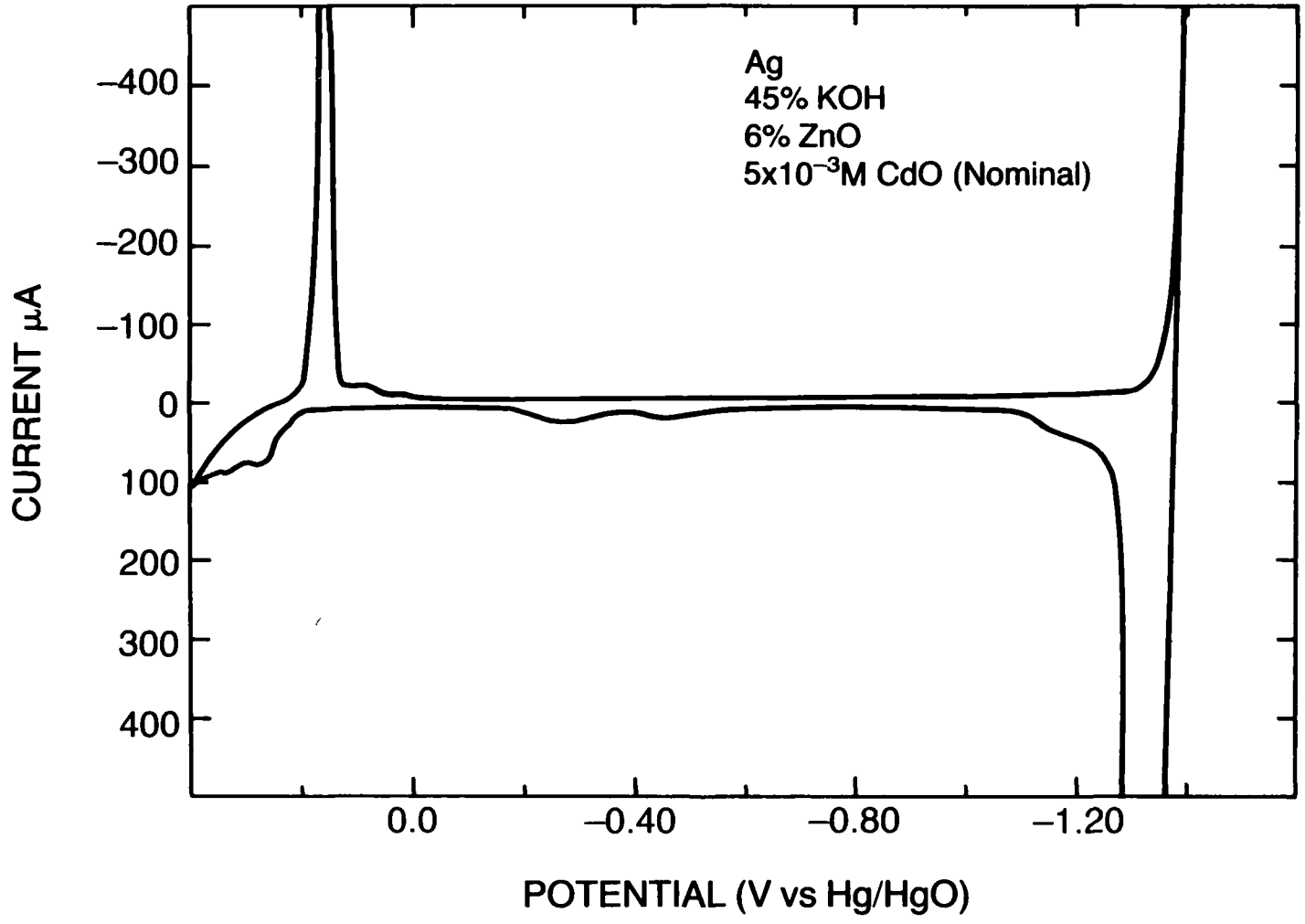
Ag
45% KOH
6% ZnO
5x10⁻³M CdO (Nominal)
CURRENT μA
−400
−300
−200
−100
0
100
200
300
400
0.0
−0.40
−0.80
−1.20
POTENTIAL (V vs Hg/HgO)

Figure 4

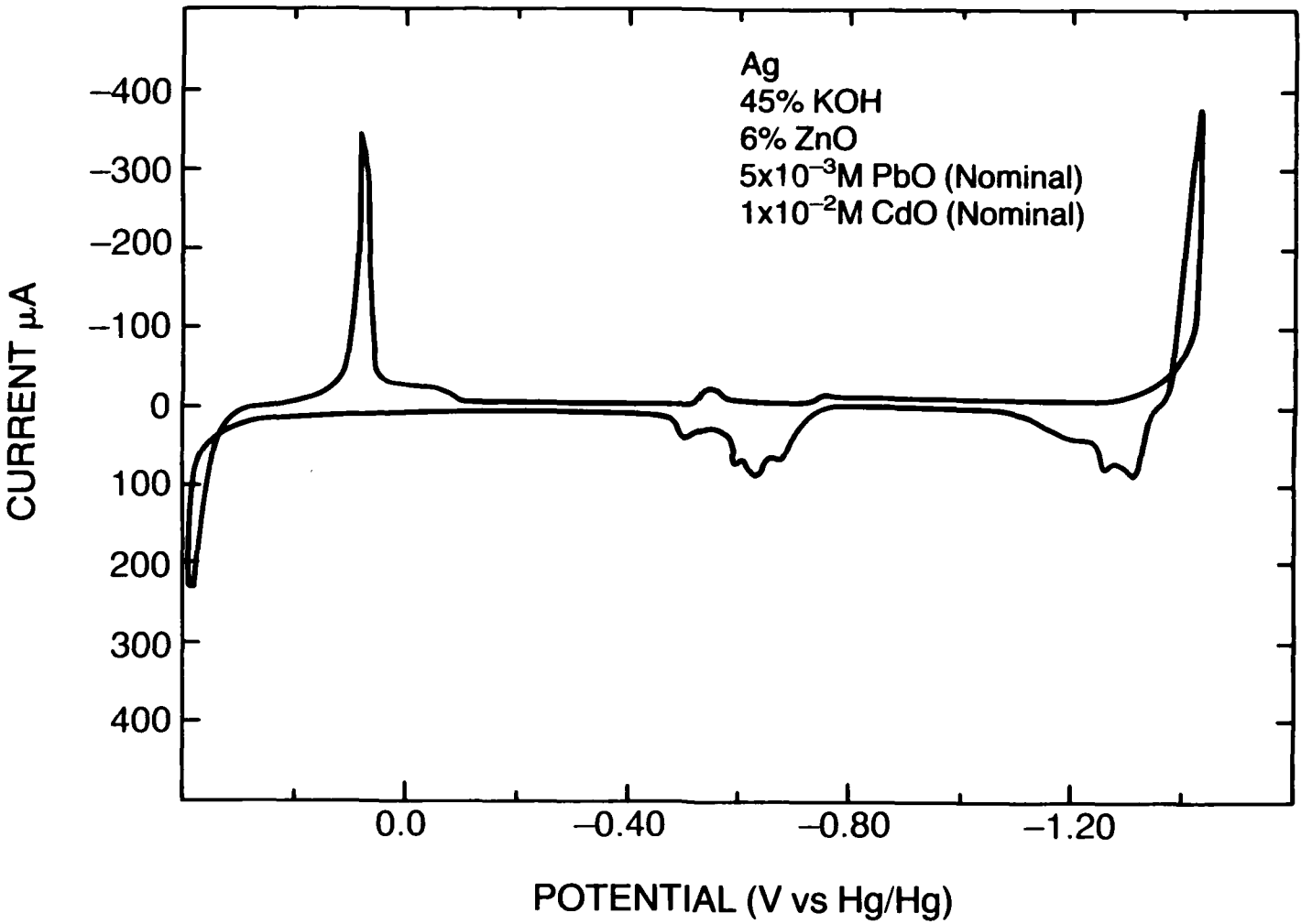
Ag
45% KOH
6% ZnO
5x10⁻³M PbO (Nominal)
1x10⁻²M CdO (Nominal)
CURRENT μA
-400
-300
-200
-100
0
100
200
300
400
0.0
-0.40
-0.80
-1.20
POTENTIAL (V vs Hg/Hg)

Figure 5

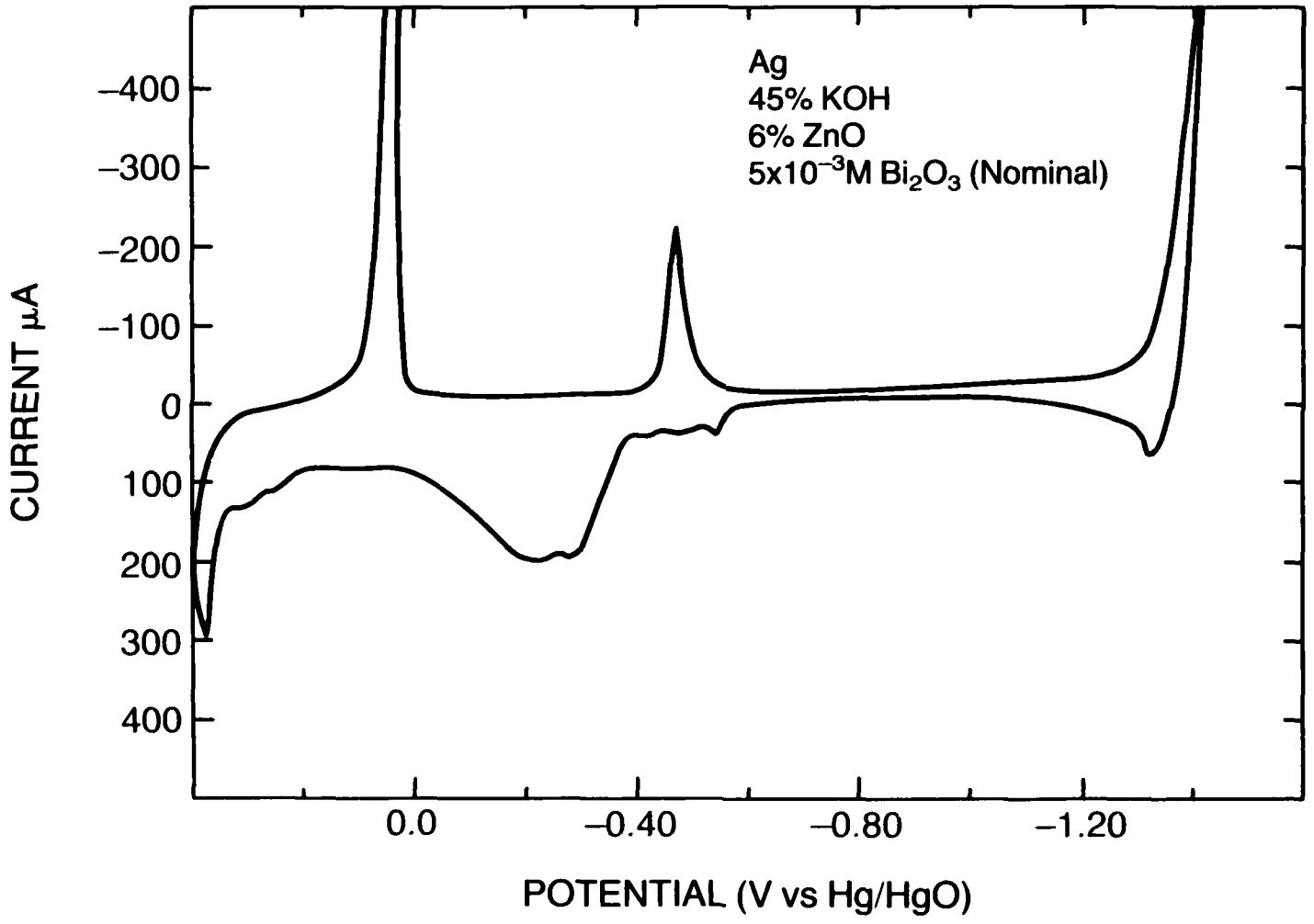
Ag
45% KOH
6% ZnO
5x10⁻³M Bi₂O₃ (Nominal)
CURRENT μA
-400
-300
-200
-100
0
100
200
300
400
0.0
-0.40
-0.80
-1.20
POTENTIAL (V vs Hg/HgO)

Figure 6

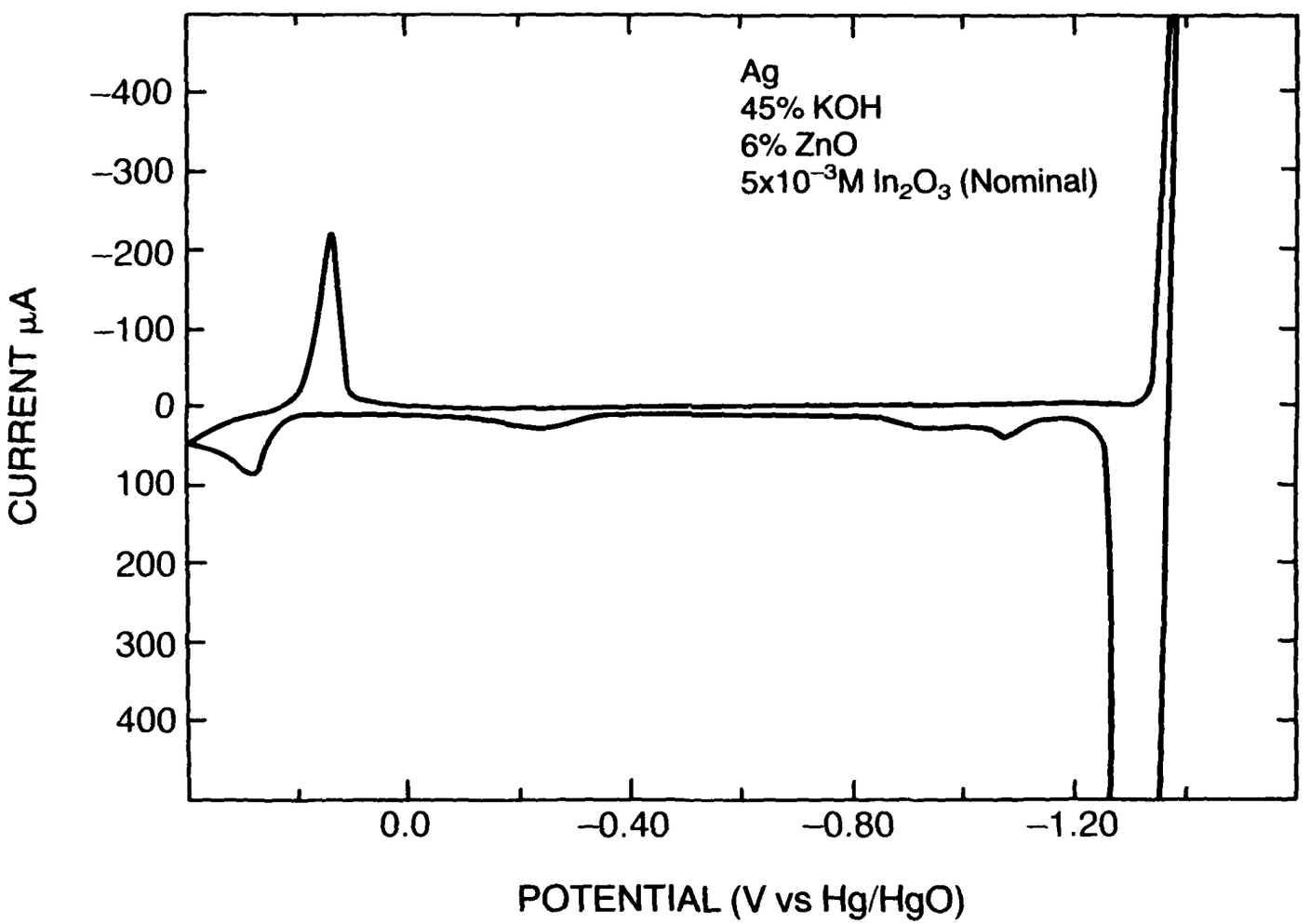
Ag
45% KOH
6% ZnO
5x10⁻³M In₂O₃ (Nominal)
CURRENT μA
-400
-300
-200
-100
0
100
200
300
400
0.0
-0.40
-0.80
-1.20
POTENTIAL (V vs Hg/HgO)

Figure 7

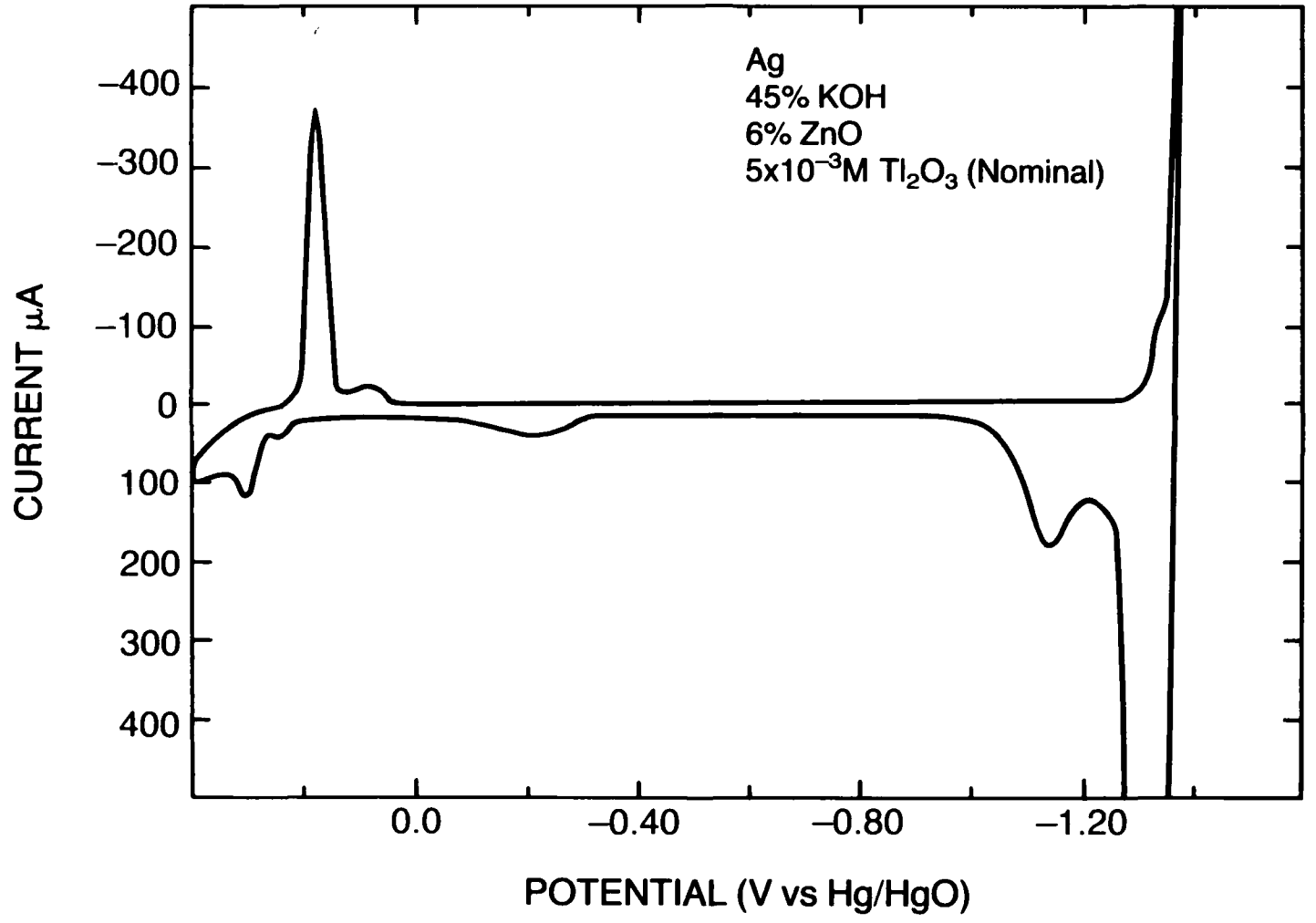
Ag
45% KOH
6% ZnO
5x10⁻³M Tl₂O₃ (Nominal)
CURRENT μA
−400
−300
−200
−100
0
100
200
300
400
0.0
−0.40
−0.80
−1.20
POTENTIAL (V vs Hg/HgO)

Figure 8

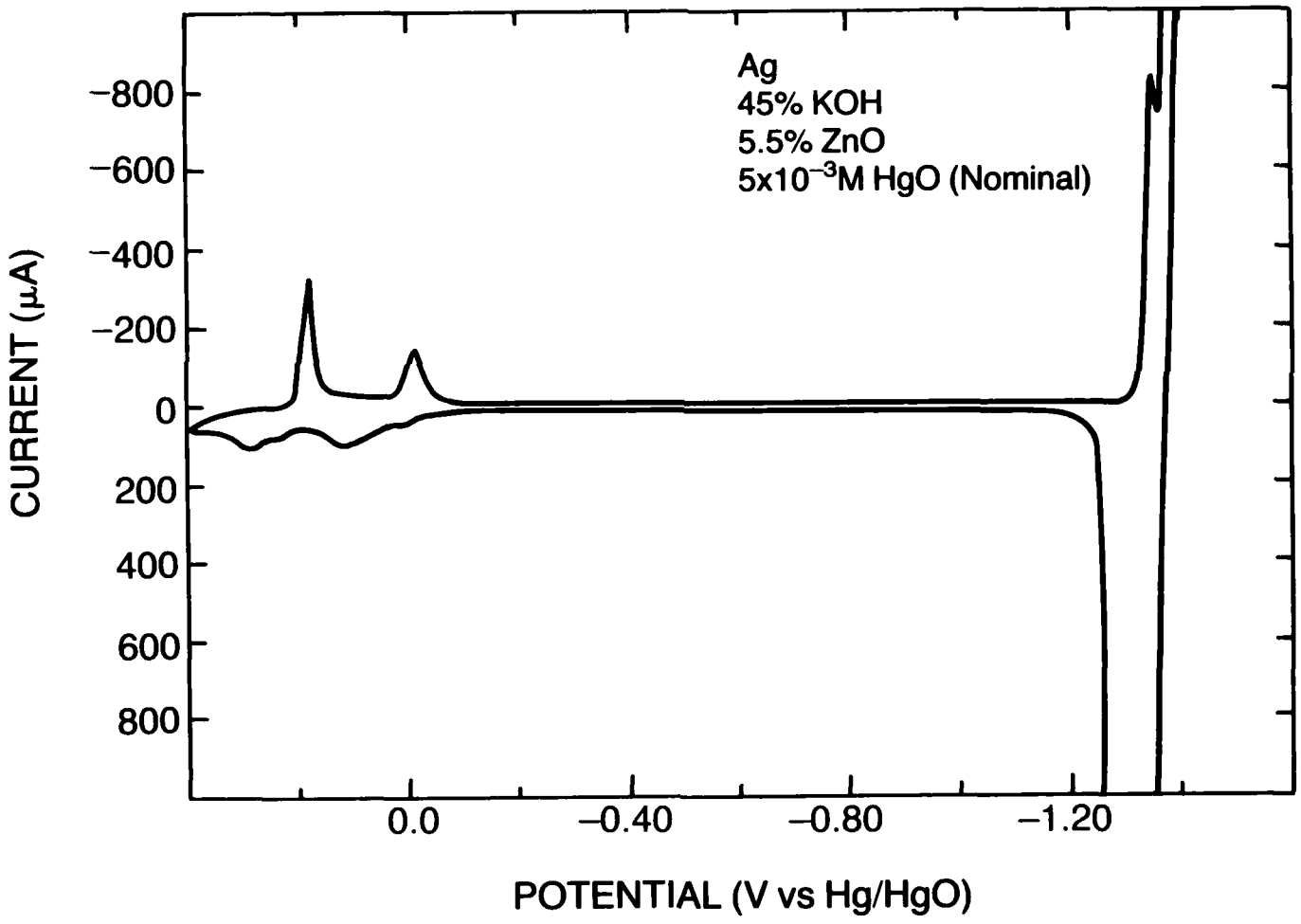
Ag
45% KOH
5.5% ZnO
5x10⁻³M HgO (Nominal)
CURRENT (μA)
−800
−600
−400
−200
0
200
400
600
800
0.0
−0.40
−0.80
−1.20
POTENTIAL (V vs Hg/HgO)

Figure 9

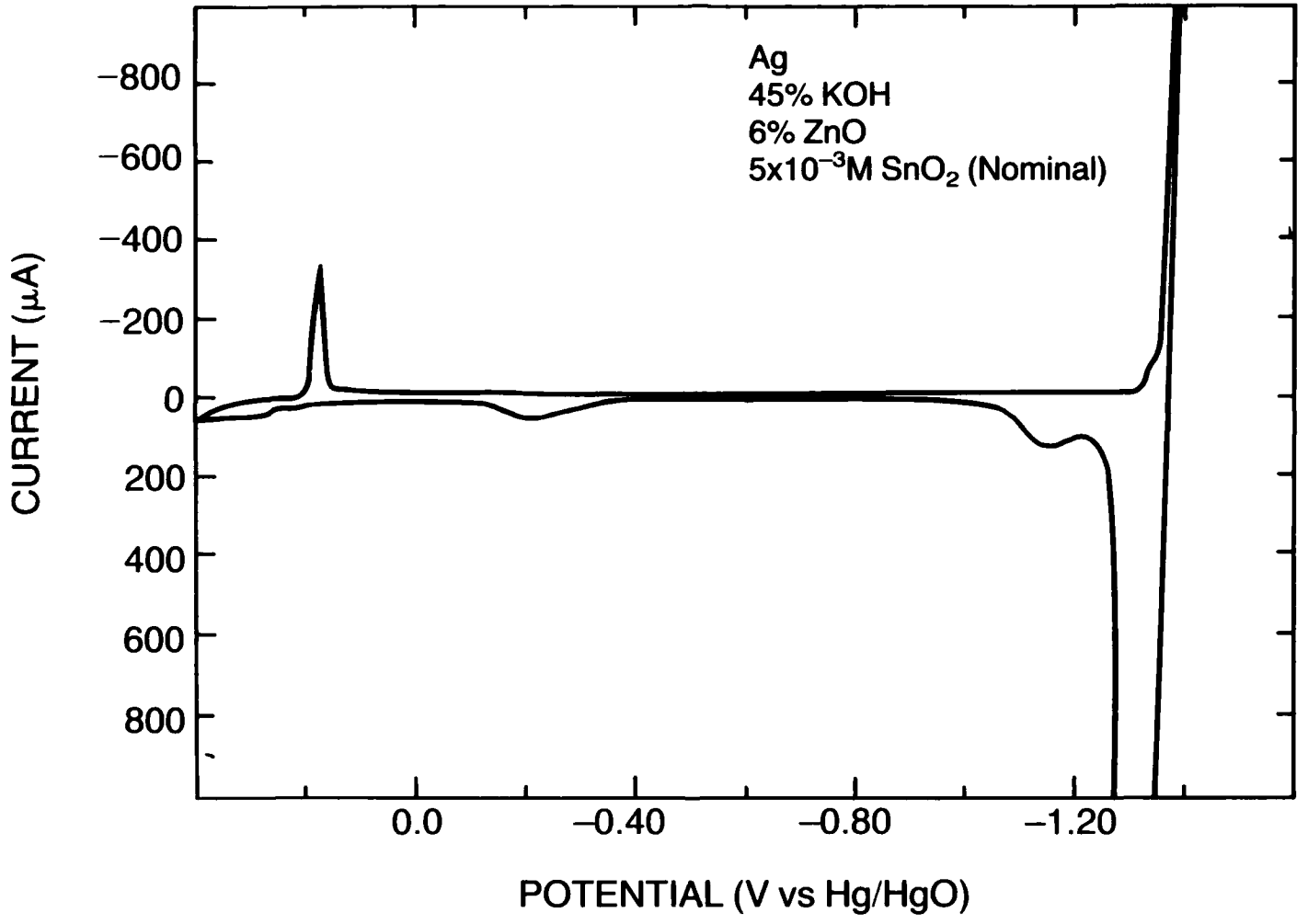
Ag
45% KOH
6% ZnO
5x10⁻³M SnO₂ (Nominal)
CURRENT (μA)
−800
−600
−400
−200
0
200
400
600
800
0.0
−0.40
−0.80
−1.20
POTENTIAL (V vs Hg/HgO)

Figure 10

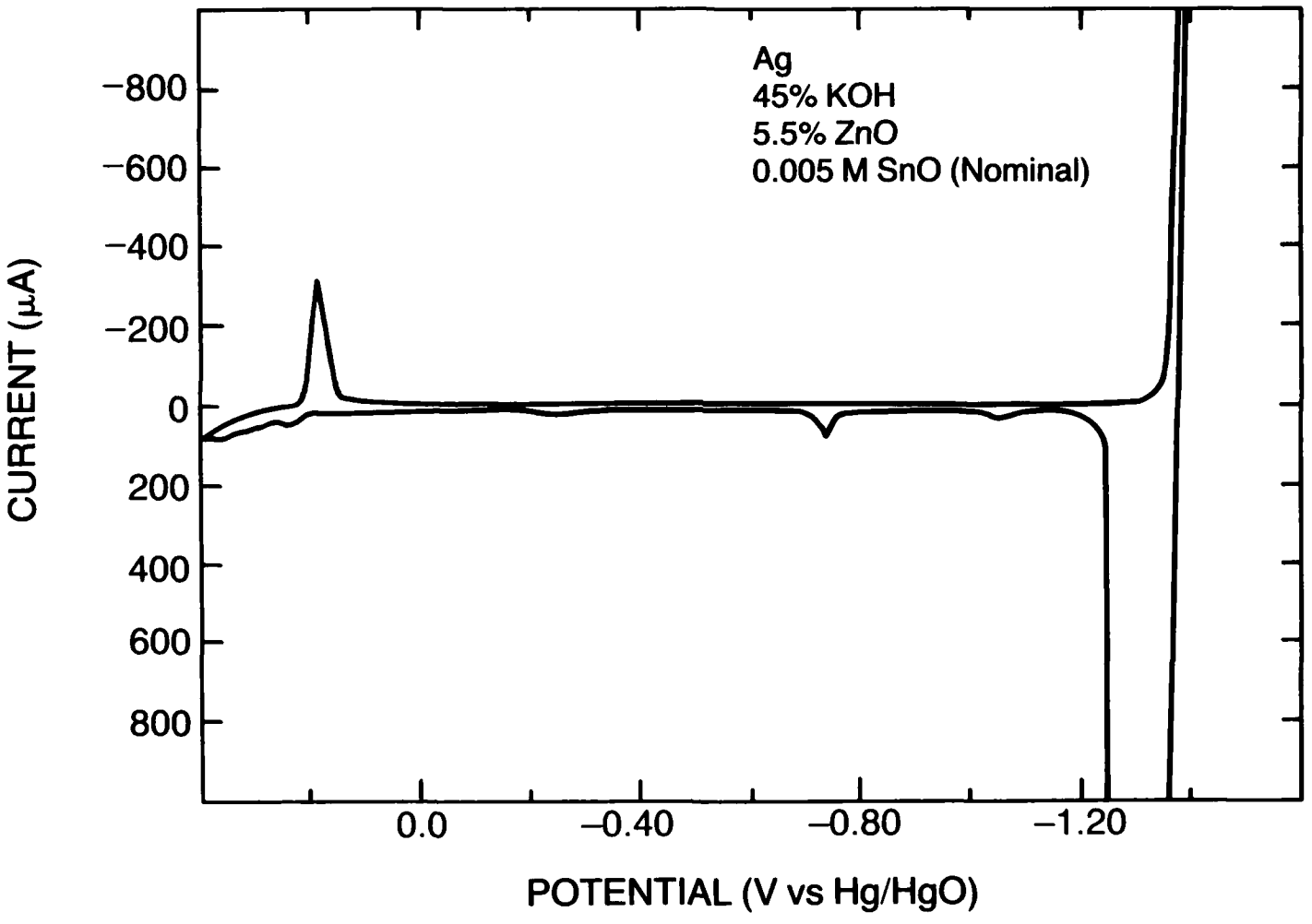
Ag
45% KOH
5.5% ZnO
0.005 M SnO (Nominal)
CURRENT (μA)
−800
−600
−400
−200
0
200
400
600
800
0.0
−0.40
−0.80
−1.20
POTENTIAL (V vs Hg/HgO)

Figure 11

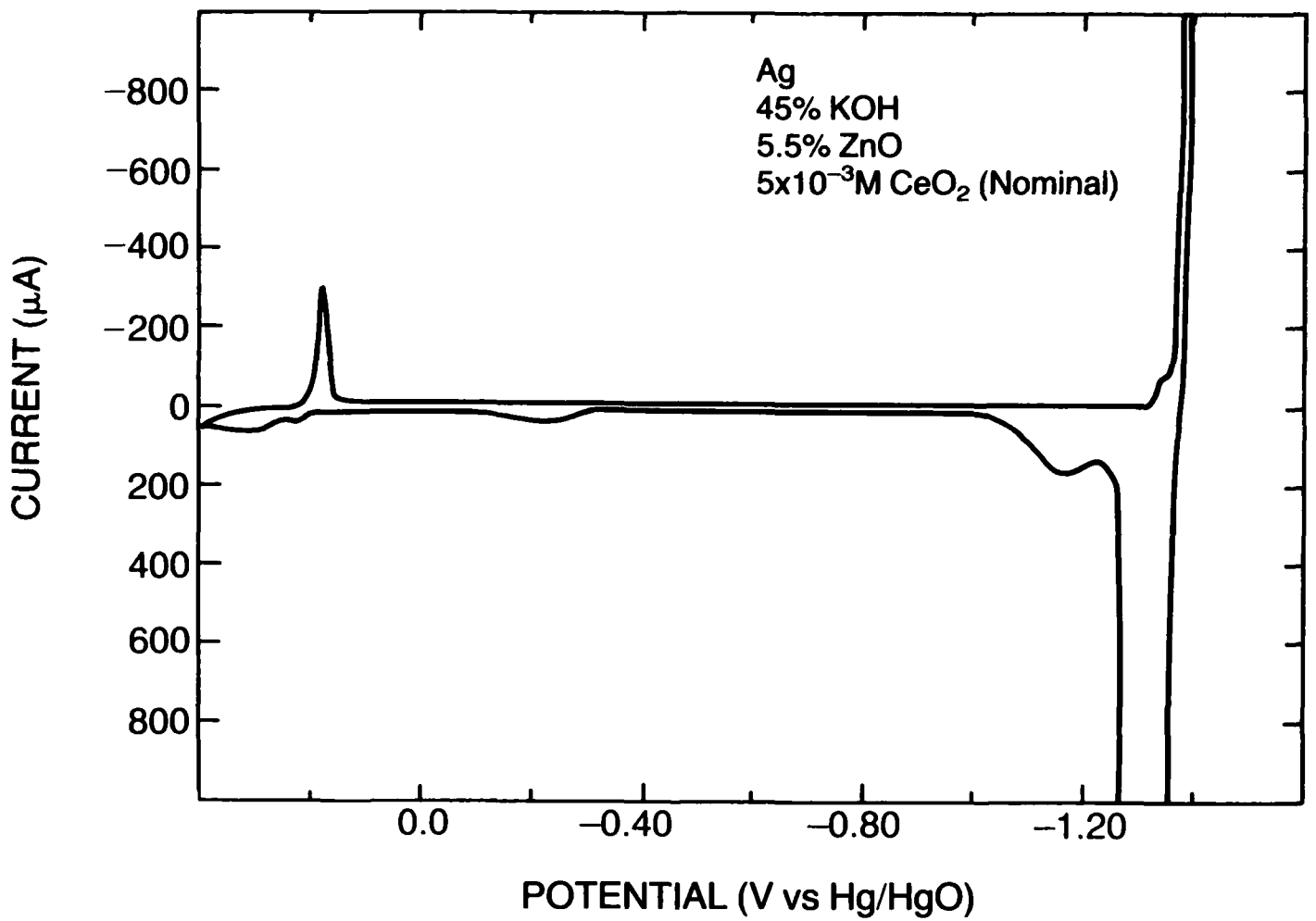
Ag
45% KOH
5.5% ZnO
5x10⁻³M CeO₂ (Nominal)
CURRENT (μA)
−800
−600
−400
−200
0
200
400
600
800
0.0
−0.40
−0.80
−1.20
POTENTIAL (V vs Hg/HgO)

Figure 12

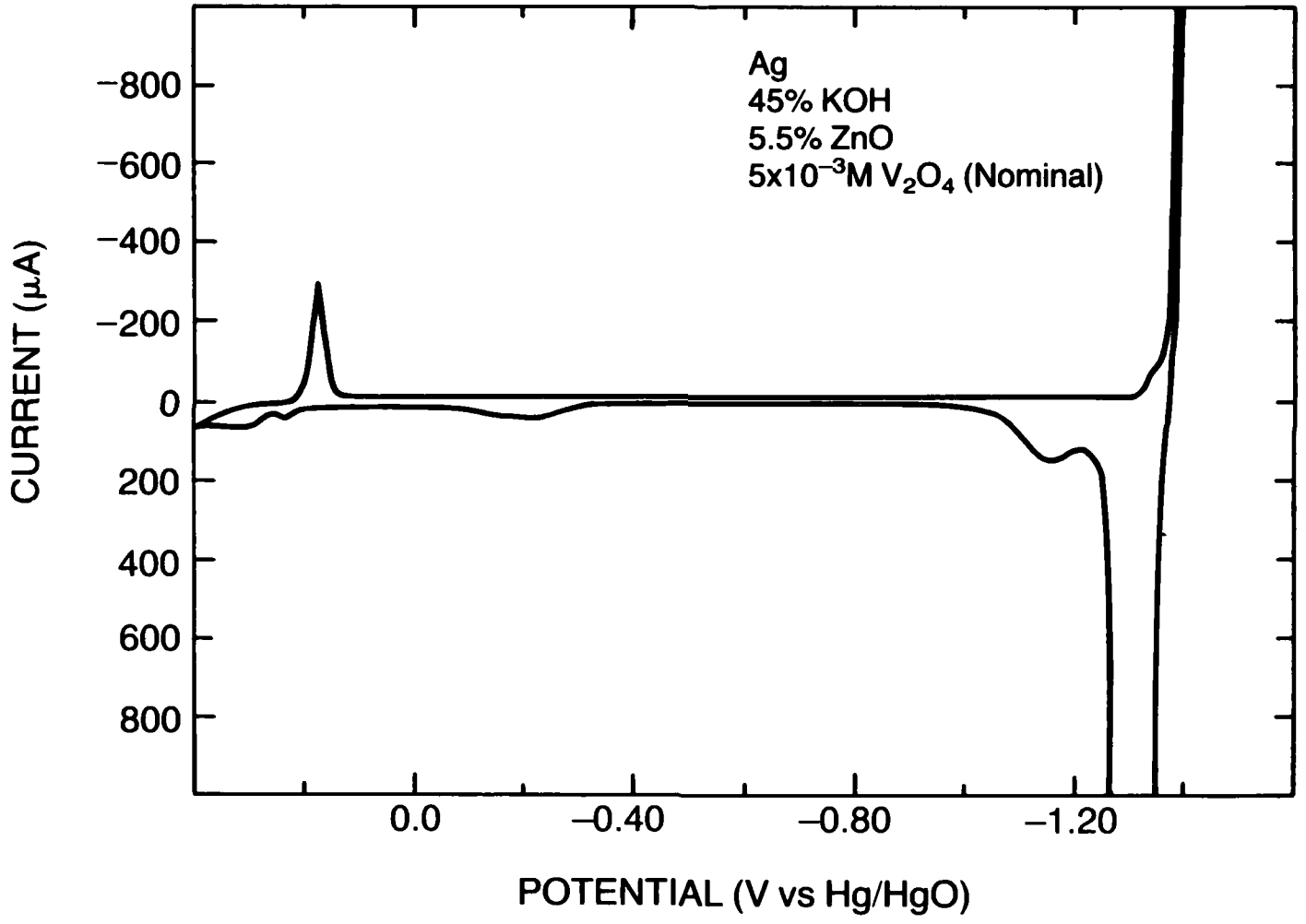
Ag
45% KOH
5.5% ZnO
5x10⁻³M V₂O₄ (Nominal)
CURRENT (μA)
−800
−600
−400
−200
0
200
400
600
800
0.0
−0.40
−0.80
−1.20
POTENTIAL (V vs Hg/HgO)

Figure 13

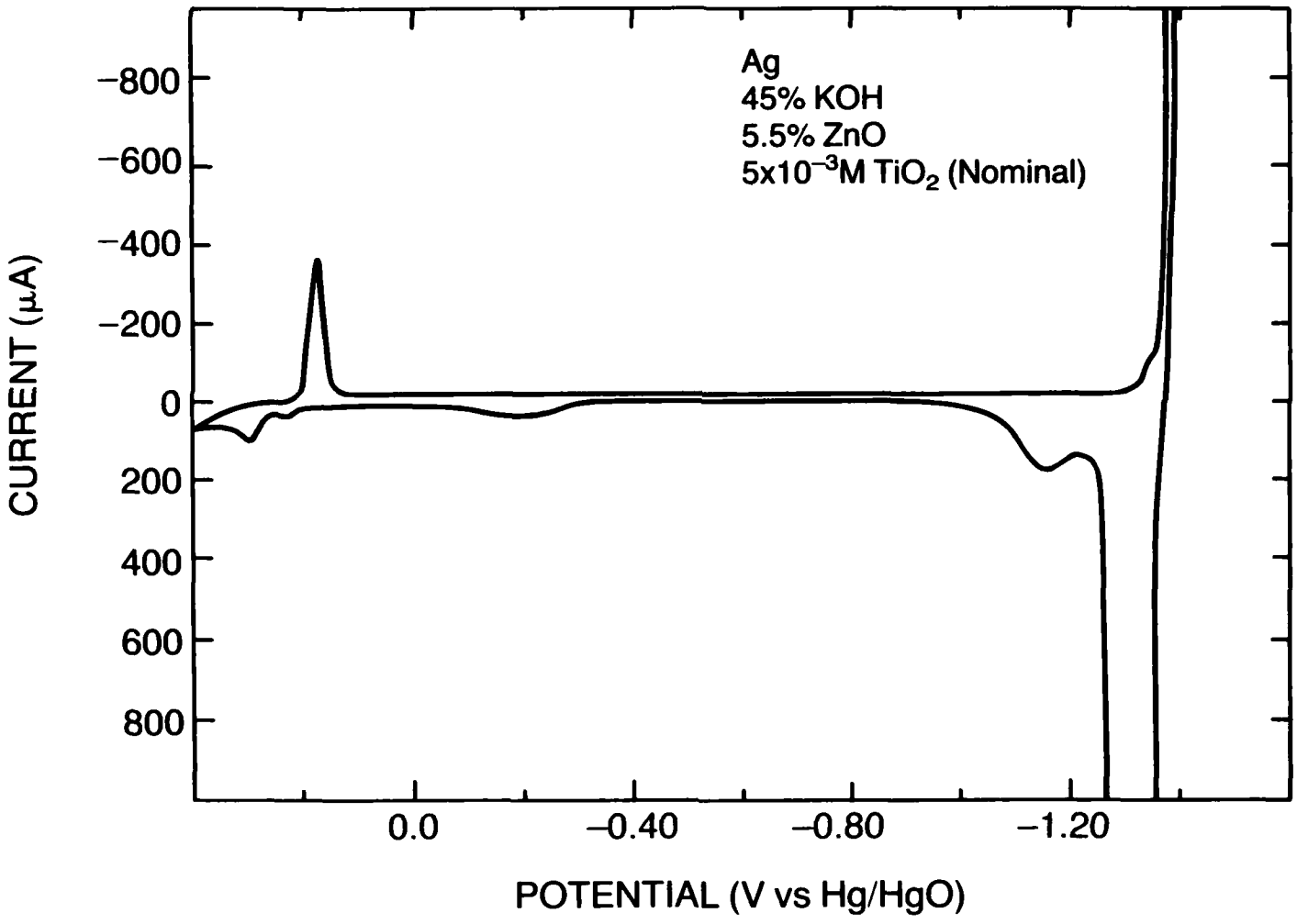
Ag
45% KOH
5.5% ZnO
5x10⁻³M TiO₂ (Nominal)
CURRENT (μA)
−800
−600
−400
−200
0
200
400
600
800
0.0
−0.40
−0.80
−1.20
POTENTIAL (V vs Hg/HgO)

Figure 14

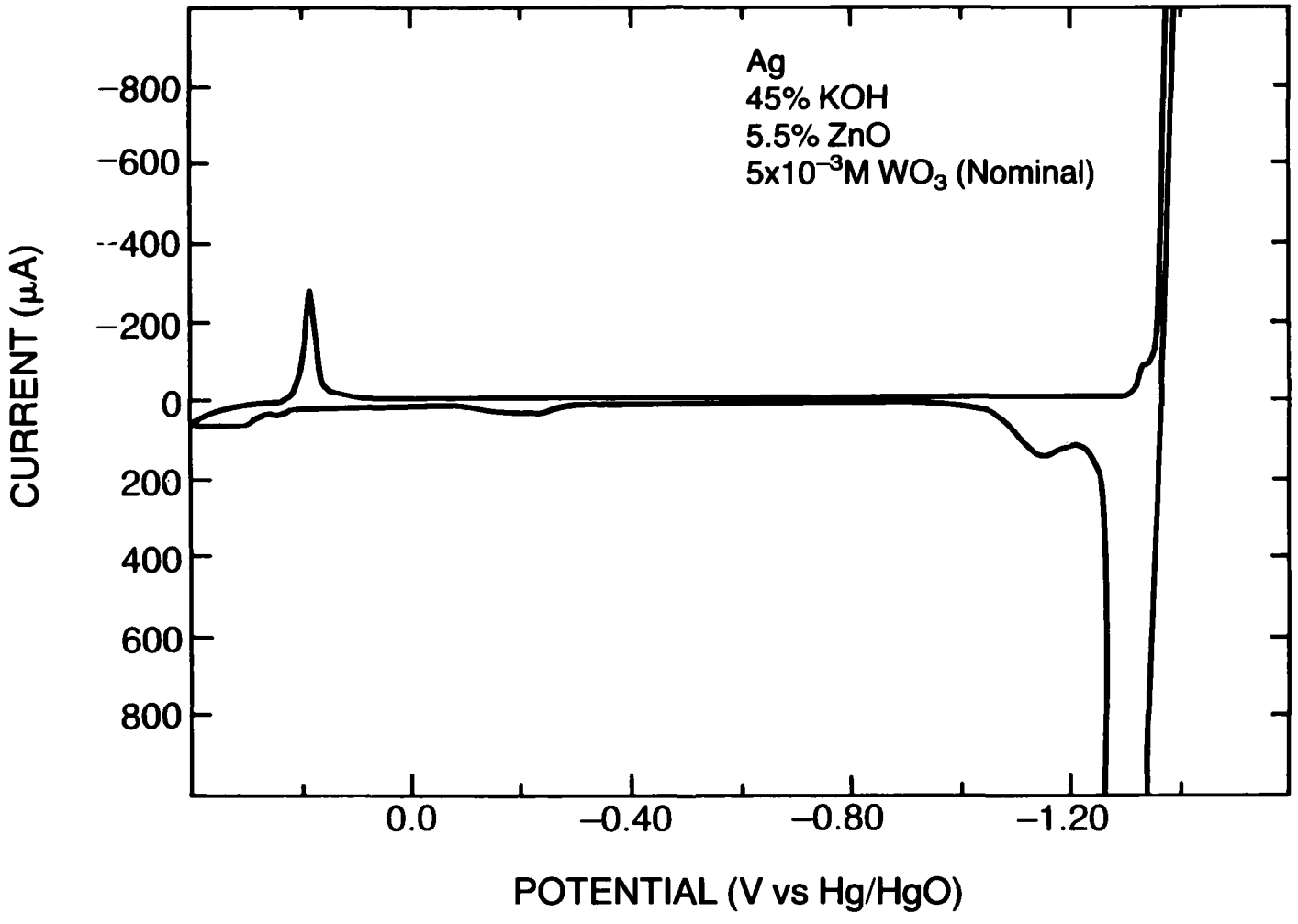
Ag
45% KOH
5.5% ZnO
5x10⁻³M WO₃ (Nominal)
CURRENT (μA)
-800
-600
-400
-200
0
200
400
600
800
0.0
-0.40
-0.80
-1.20
POTENTIAL (V vs Hg/HgO)

Figure 15

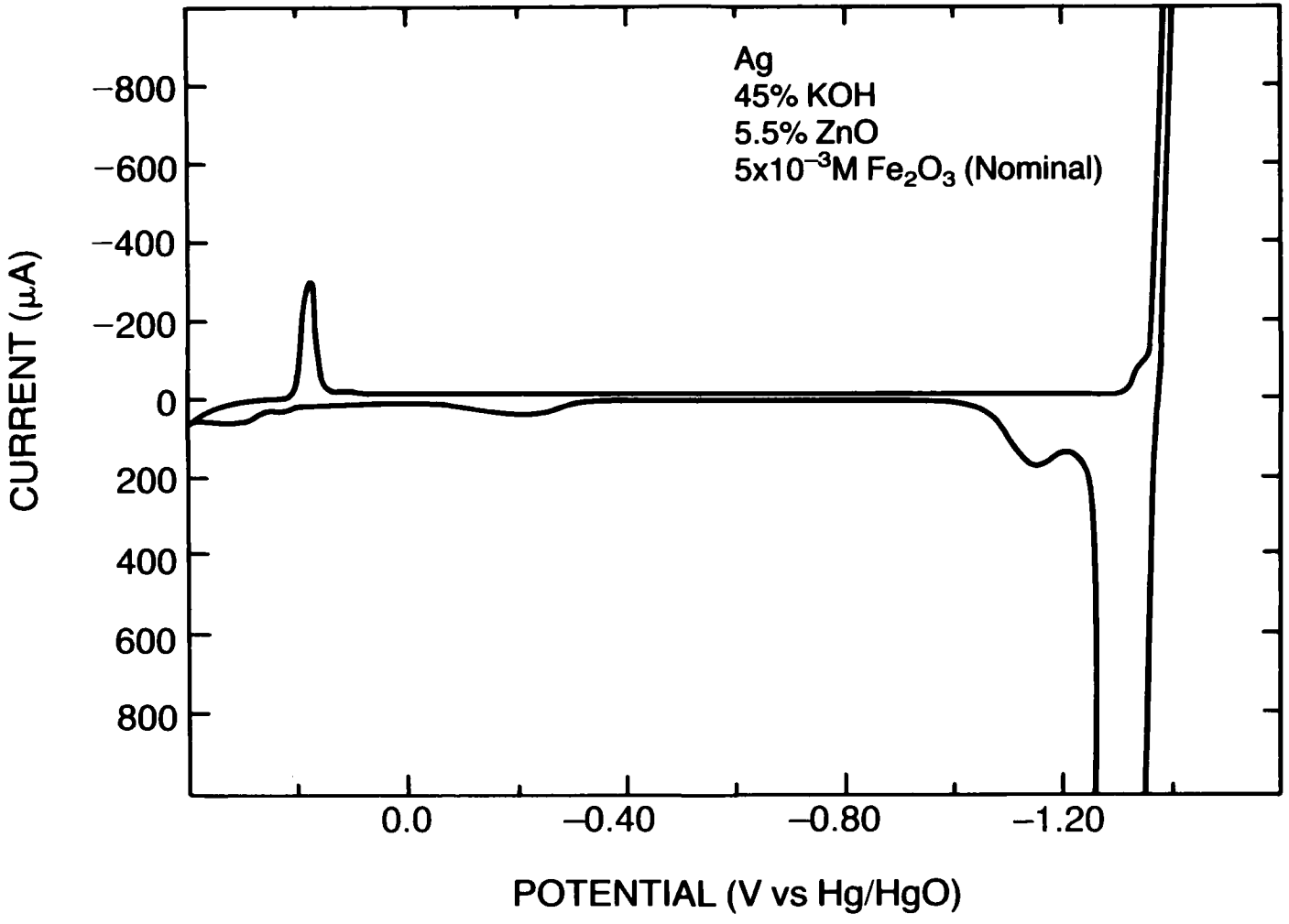
Ag
45% KOH
5.5% ZnO
5x10⁻³M Fe₂O₃ (Nominal)
CURRENT (μA)
−800
−600
−400
−200
0
200
400
600
800
0.0
−0.40
−0.80
−1.20
POTENTIAL (V vs Hg/HgO)

Figure 16

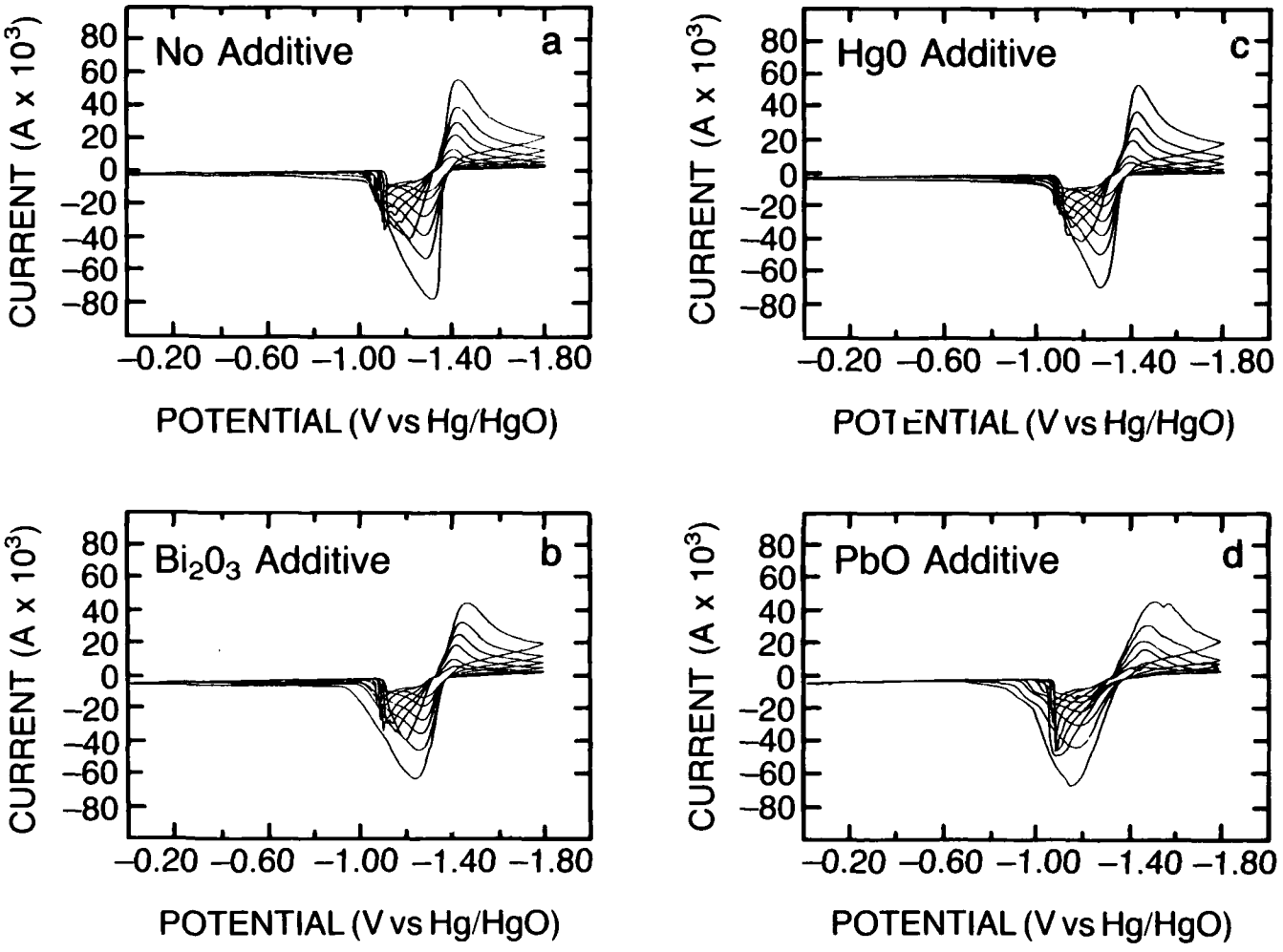
No Additive
a
Hg0 Additive
c
Bi_2O_3 Additive
b
PbO Additive
d
CURRENT (A x 10^3)
80
60
40
20
0
−20
−40
−60
−80
−0.20 −0.60 −1.00 −1.40 −1.80
POTENTIAL (V vs Hg/HgO)

Figure 17

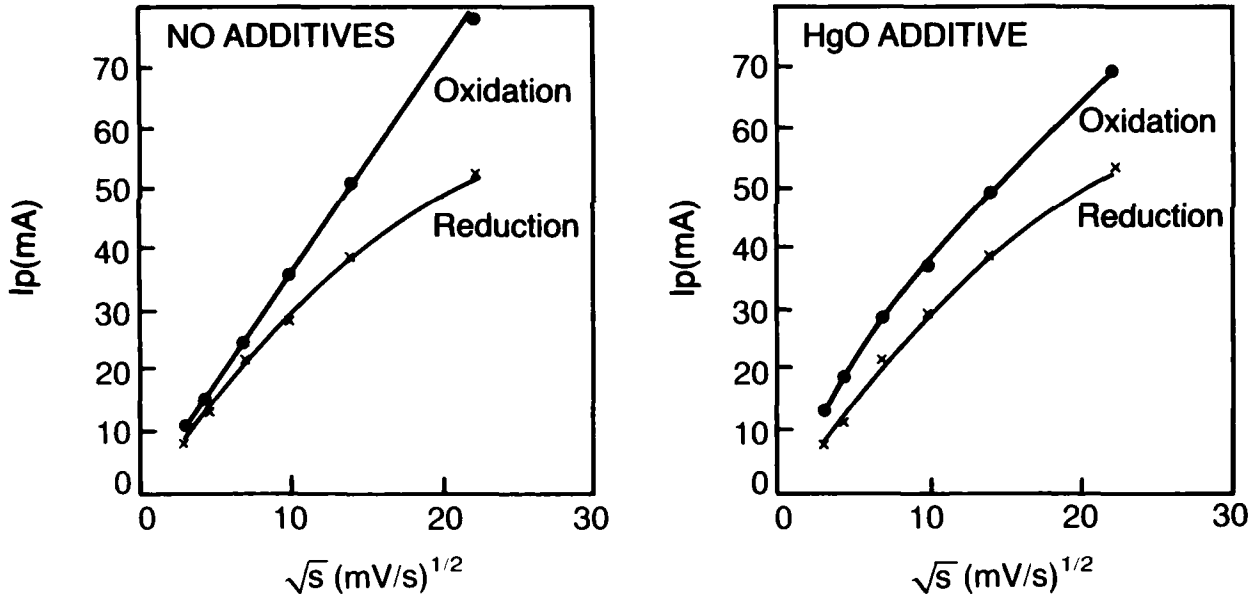
NO ADDITIVES
Oxidation
Reduction
Ip(mA)
70
60
50
40
30
20
10
0
0
10
20
30
√s (mV/s)^1/2
HgO ADDITIVE
Oxidation
Reduction
Ip(mA)
70
60
50
40
30
20
10
0
0
10
20
30
√s (mV/s)^1/2

Figure 18

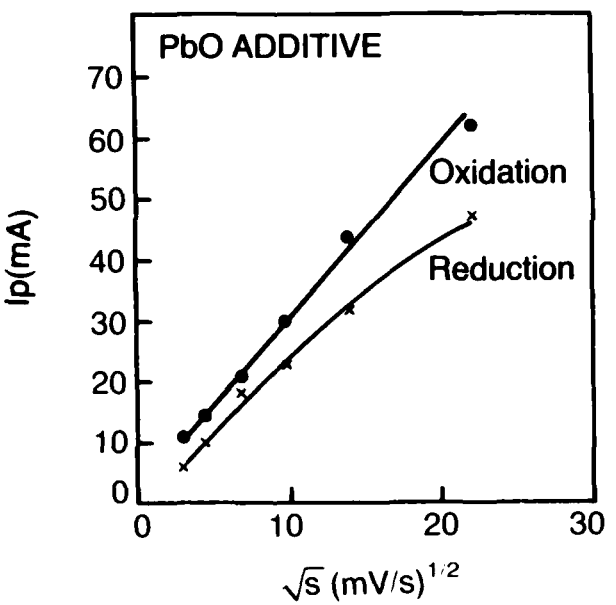
PbO ADDITIVE
Oxidation
Reduction
Ip(mA)
70
60
50
40
30
20
10
0
0
10
20
30
√s (mV/s)^1/2

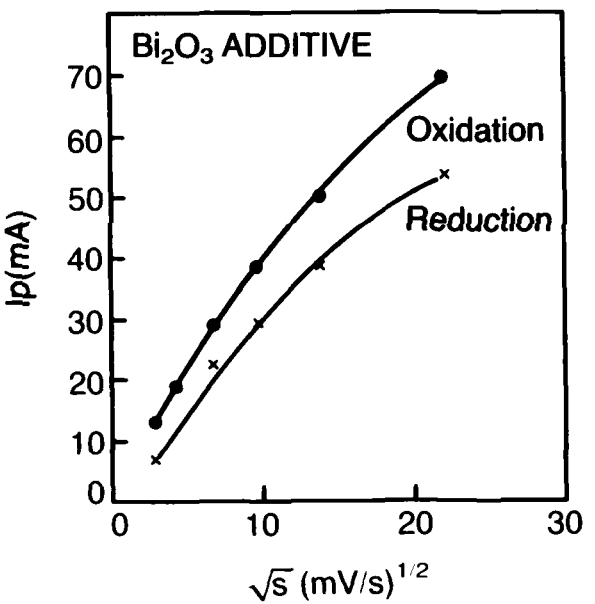
Bi2O3 ADDITIVE
Oxidation
Reduction
Ip(mA)
70
60
50
40
30
20
10
0
0
10
20
30
√s (mV/s)^1/2

Figure 19

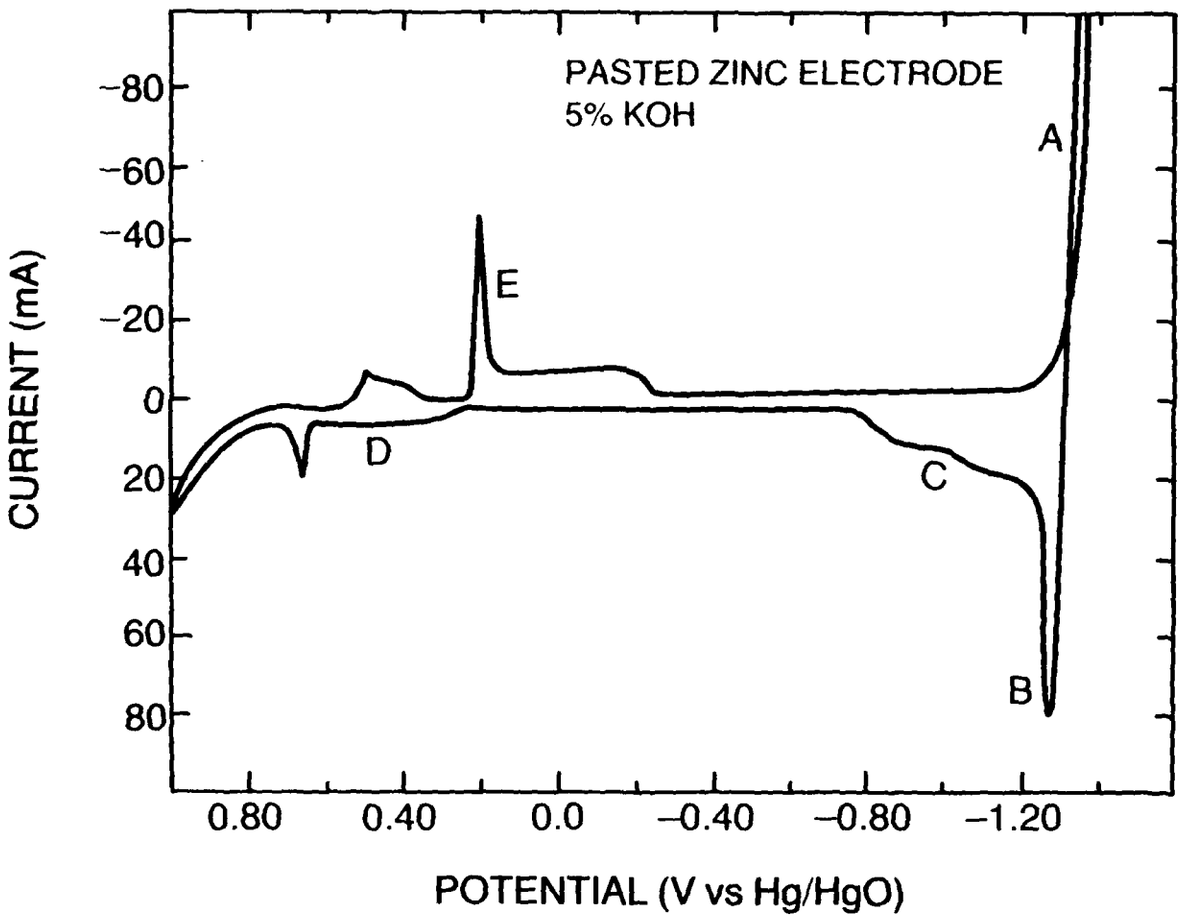
PASTED ZINC ELECTRODE
5% KOH
A
B
C
D
E
CURRENT (mA)
−80
−60
−40
−20
0
20
40
60
80
0.80
0.40
0.0
−0.40
−0.80
−1.20
POTENTIAL (V vs Hg/HgO)

Figure 20

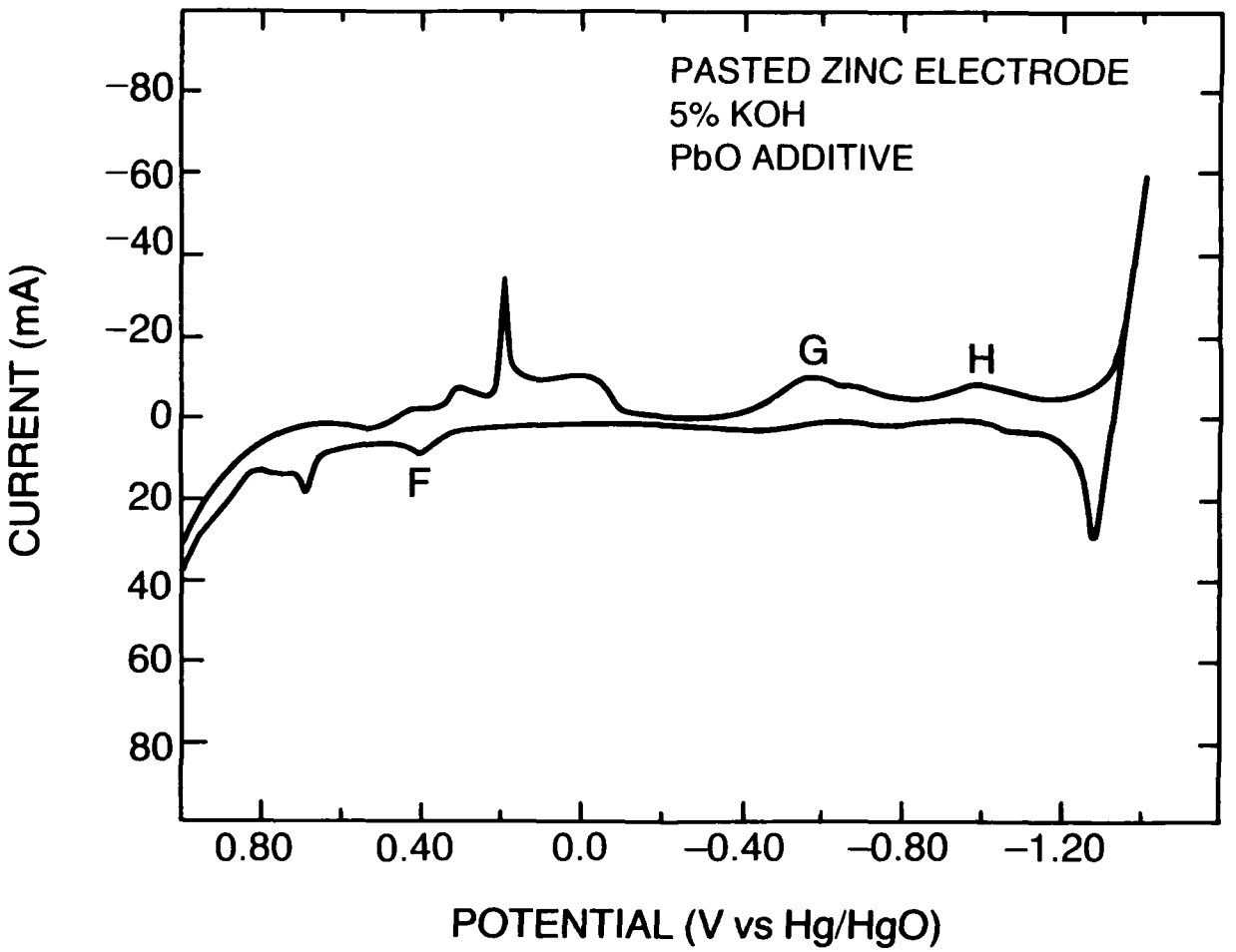
PASTED ZINC ELECTRODE
5% KOH
PbO ADDITIVE
G
H
F
CURRENT (mA)
−80
−60
−40
−20
0
20
40
60
80
0.80
0.40
0.0
−0.40
−0.80
−1.20
POTENTIAL (V vs Hg/HgO)

Figure 21

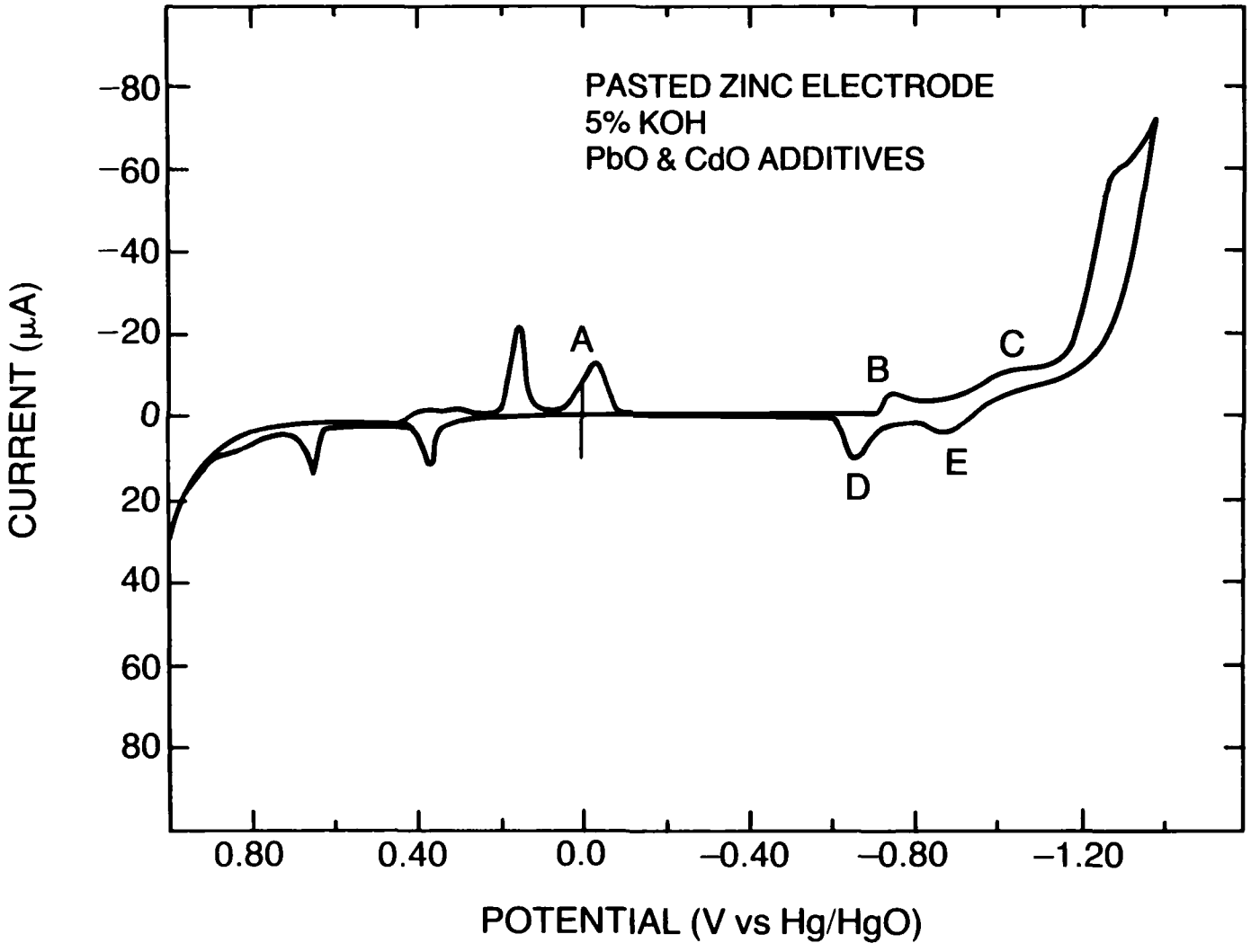
PASTED ZINC ELECTRODE
5% KOH
PbO & CdO ADDITIVES
A
B
C
D
E
−80
−60
−40
−20
0
20
40
60
80
CURRENT (μA)
0.80
0.40
0.0
−0.40
−0.80
−1.20
POTENTIAL (V vs Hg/HgO)

Figure 22

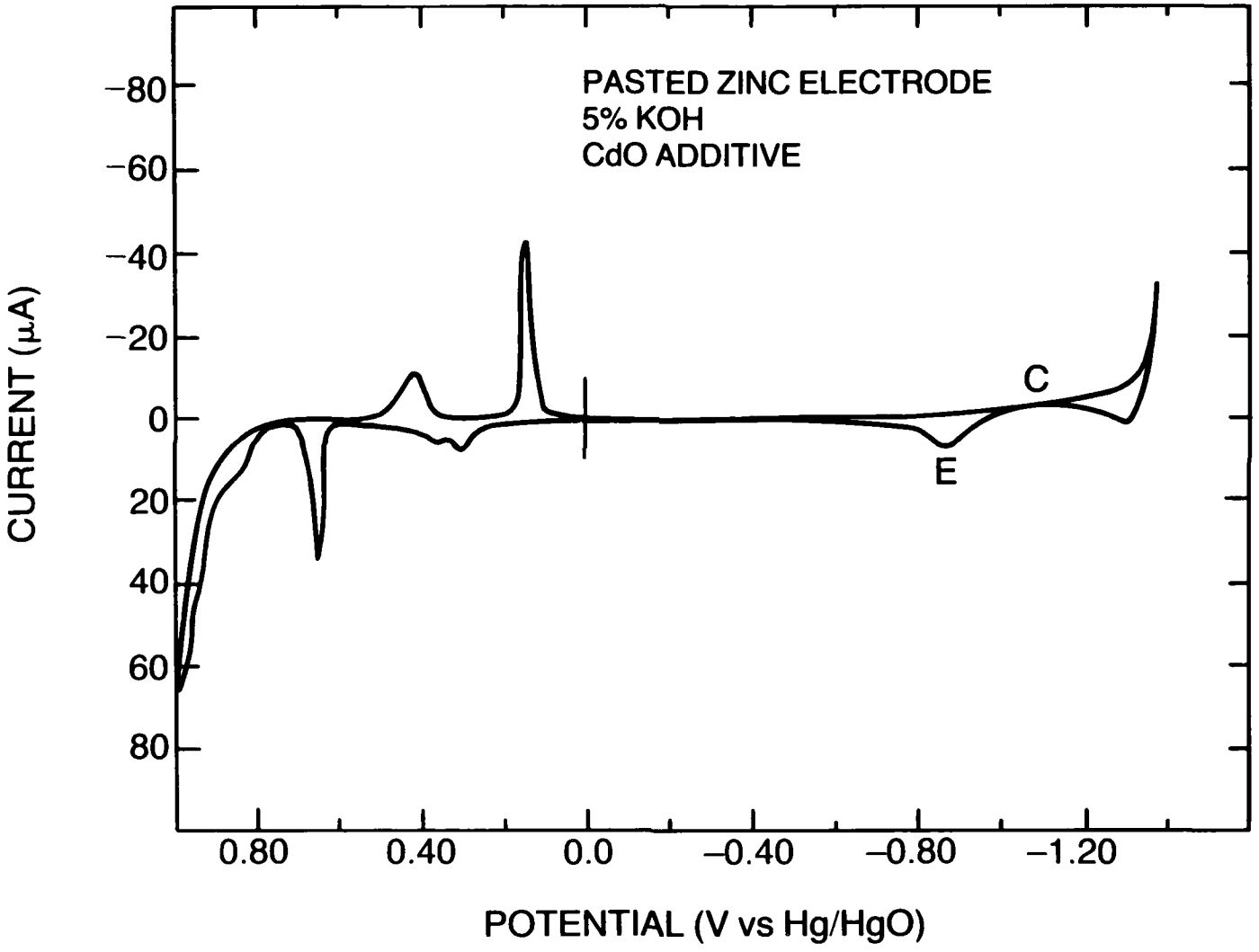
PASTED ZINC ELECTRODE
5% KOH
CdO ADDITIVE
C
E
CURRENT (μA)
−80
−60
−40
−20
0
20
40
60
80
0.80
0.40
0.0
−0.40
−0.80
−1.20
POTENTIAL (V vs Hg/HgO)

Figure 23

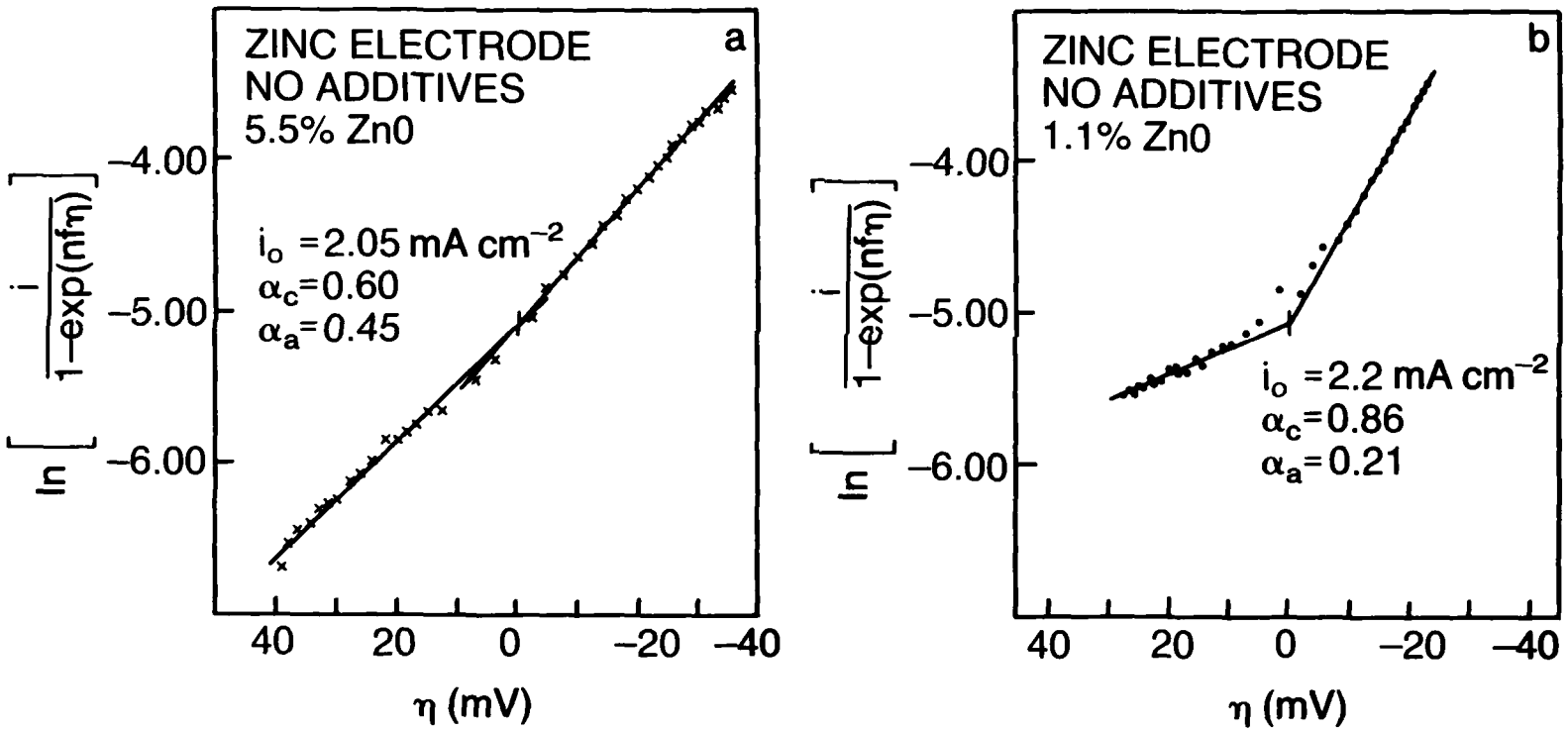
ZINC ELECTRODE
NO ADDITIVES
5.5% Zn0
a
i_o =2.05 mA cm^{-2}
α_c=0.60
α_a=0.45
ln [i / 1−exp(nfη)]
−4.00
−5.00
−6.00
40
20
0
−20
−40
η (mV)
ZINC ELECTRODE
NO ADDITIVES
1.1% Zn0
b
i_o =2.2 mA cm^{-2}
α_c=0.86
α_a=0.21
ln [i / 1−exp(nfη)]
−4.00
−5.00
−6.00
40
20
0
−20
−40
η (mV)

Figure 24

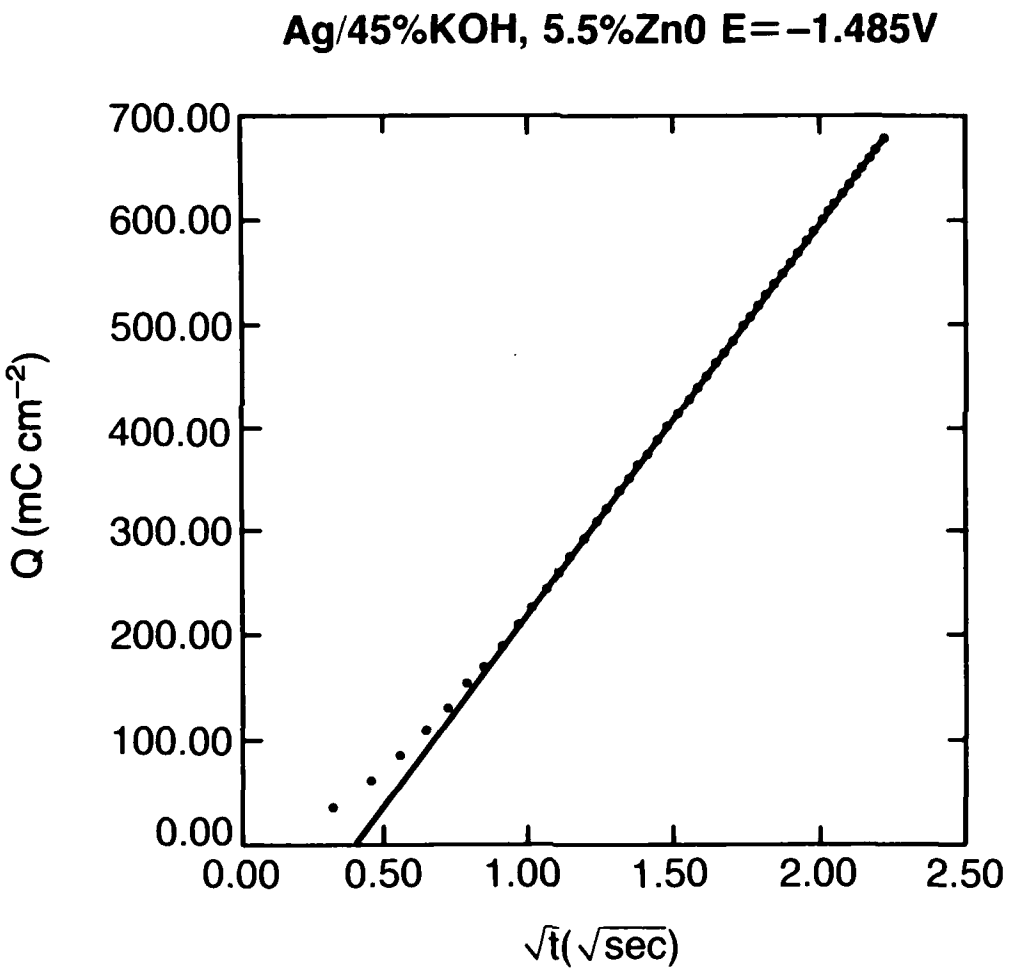
Ag/45%KOH, 5.5%Zn0 E=–1.485V
700.00
600.00
500.00
400.00
300.00
200.00
100.00
0.00
Q (mC cm^{-2})
0.00
0.50
1.00
1.50
2.00
2.50
$\sqrt{t}(\sqrt{sec})$

Figure 25

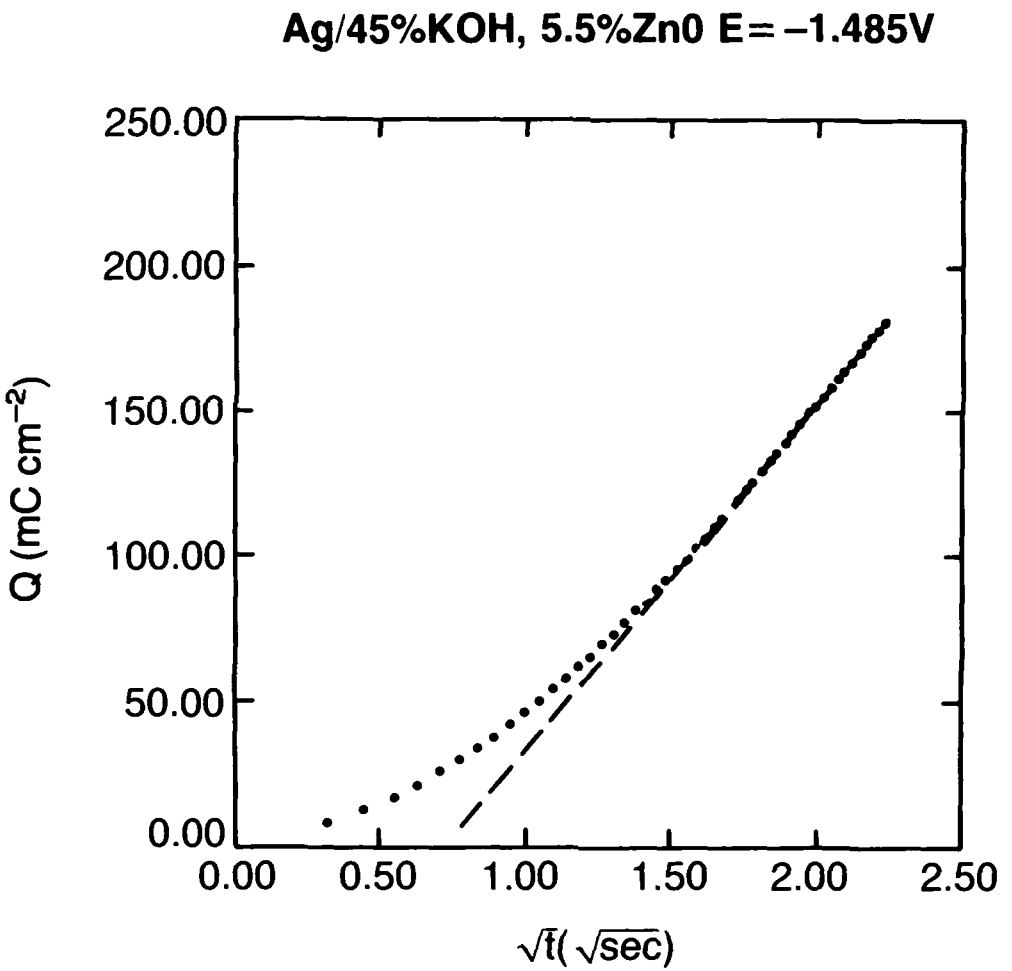
Ag/45%KOH, 5.5%Zn0 E= –1.485V
250.00
200.00
150.00
100.00
50.00
0.00
Q (mC cm^{-2})
0.00
0.50
1.00
1.50
2.00
2.50
√t(√sec)

Figure 26

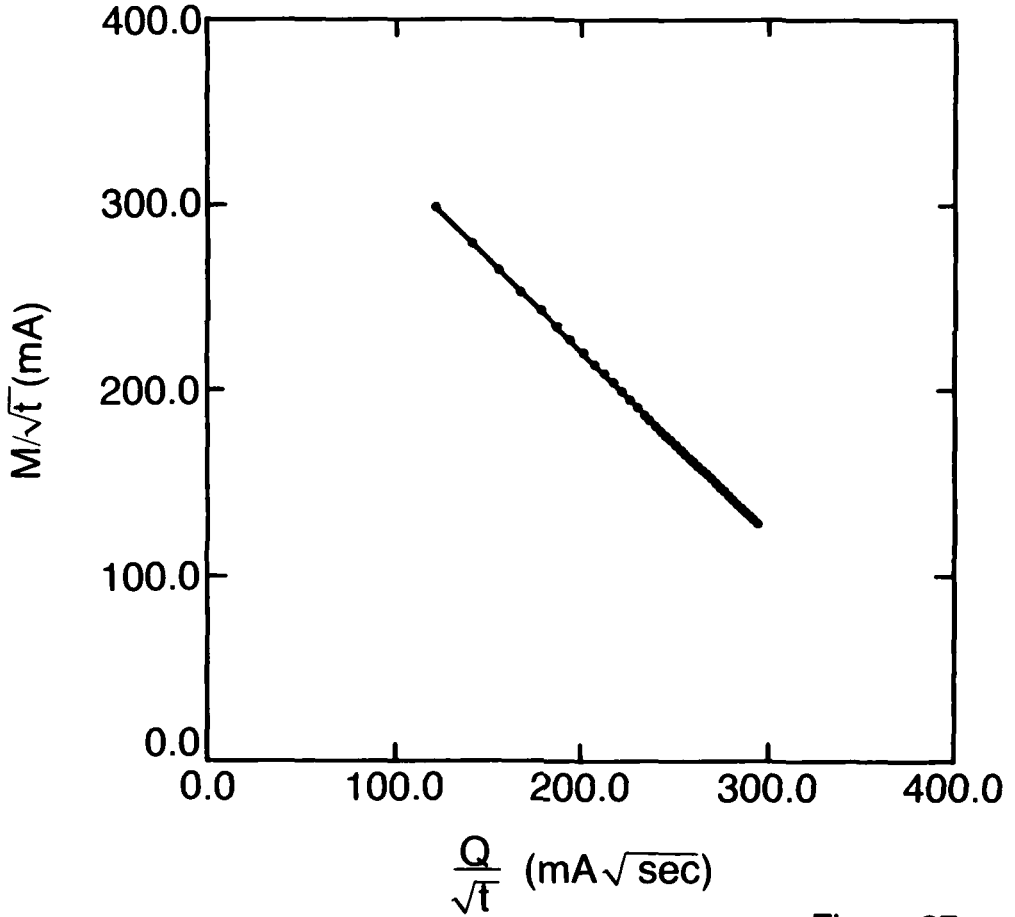

Figure 27

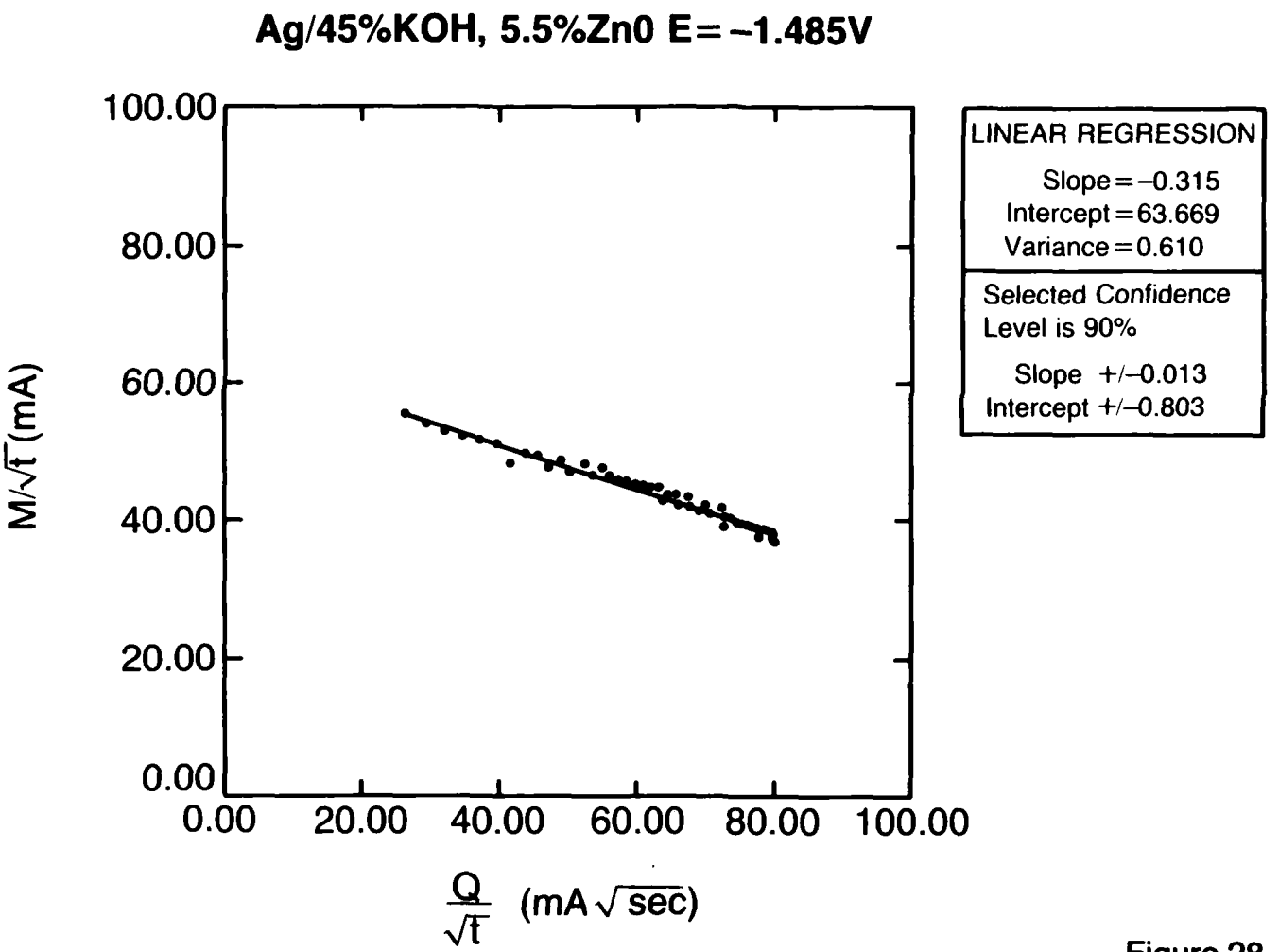
Ag/45%KOH, 5.5%Zn0 E=-1.485V
100.00
80.00
60.00
40.00
20.00
0.00
M/√t (mA)
0.00
20.00
40.00
60.00
80.00
100.00
Q/√t (mA√sec)
LINEAR REGRESSION
Slope=-0.315
Intercept=63.669
Variance=0.610
Selected Confidence Level is 90%
Slope +/-0.013
Intercept +/-0.803

Figure 28

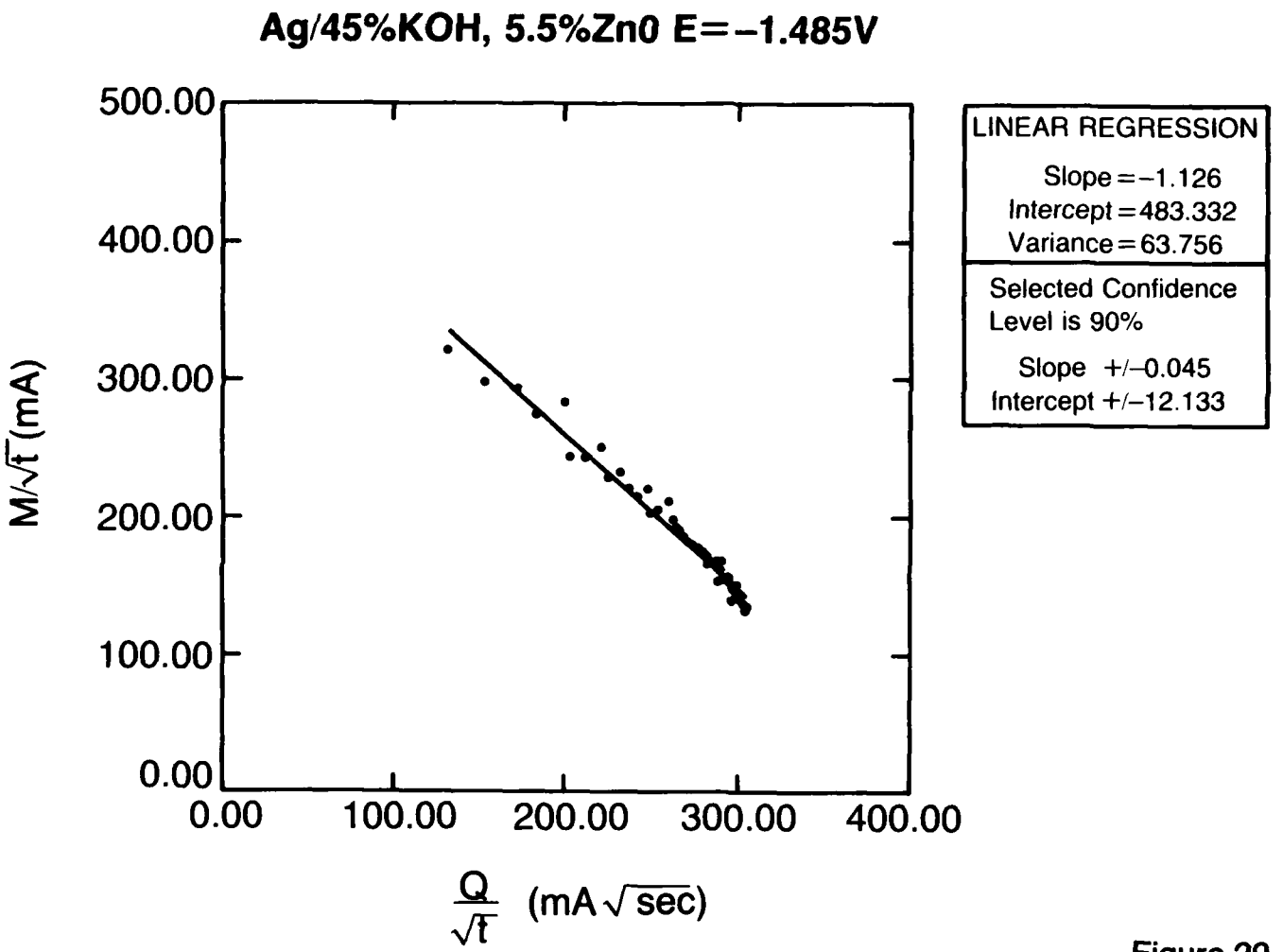
Ag/45%KOH, 5.5%Zn0 E=–1.485V
500.00
400.00
300.00
200.00
100.00
0.00
M/√t (mA)
0.00
100.00
200.00
300.00
400.00
Q/√t (mA√sec)
LINEAR REGRESSION
Slope =–1.126
Intercept =483.332
Variance =63.756
Selected Confidence Level is 90%
Slope +/–0.045
Intercept +/–12.133

Figure 29

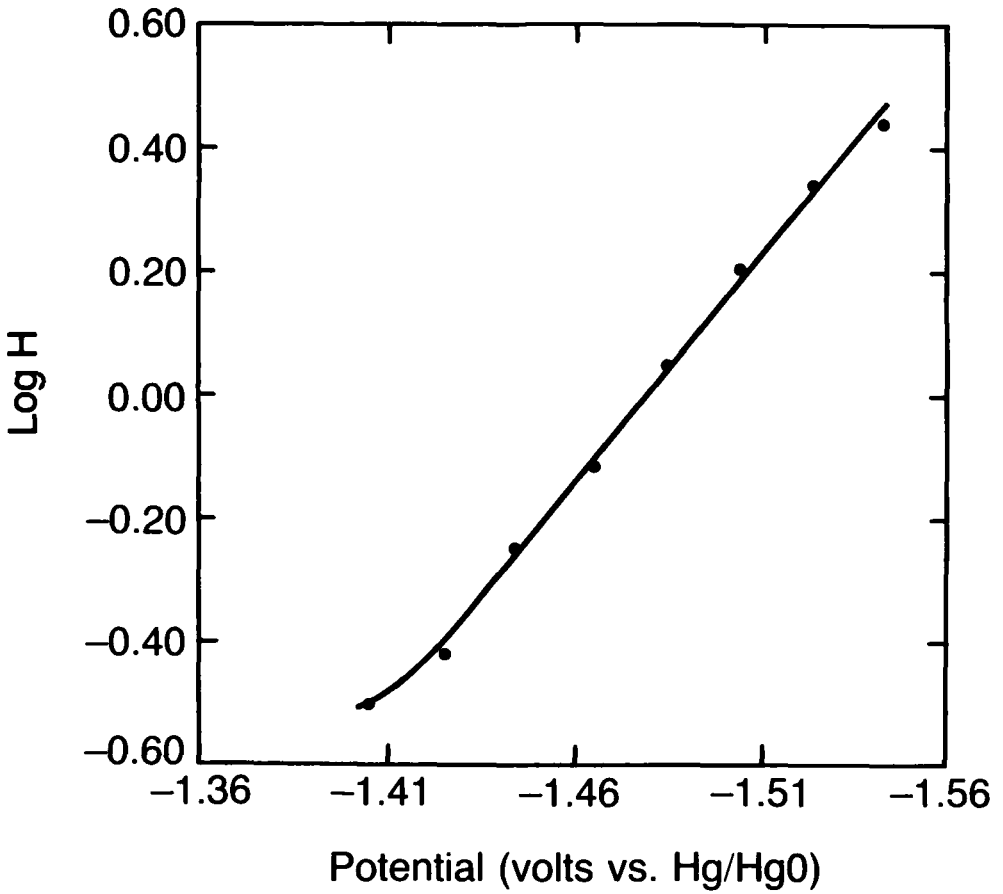
0.60
0.40
0.20
0.00
–0.20
–0.40
–0.60
Log H
–1.36
–1.41
–1.46
–1.51
–1.56
Potential (volts vs. Hg/Hg0)

Figure 30

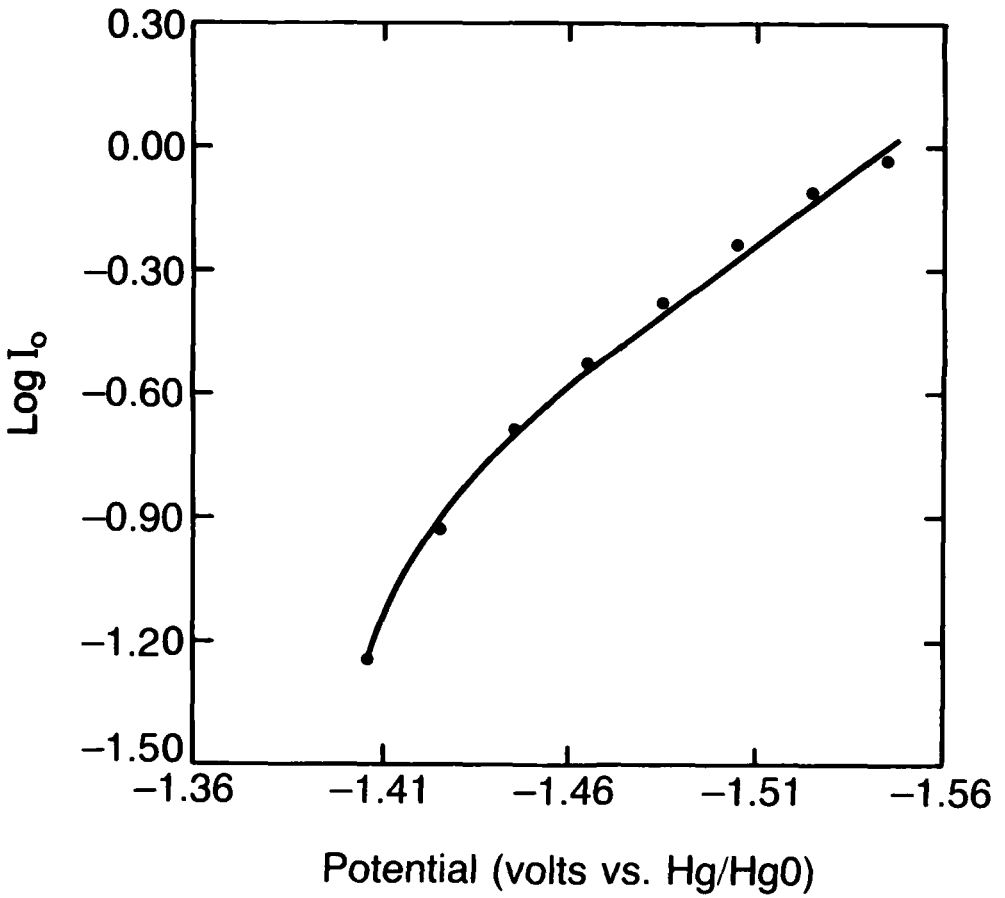
0.30
0.00
−0.30
−0.60
−0.90
−1.20
−1.50
Log I_o
−1.36
−1.41
−1.46
−1.51
−1.56
Potential (volts vs. Hg/Hg0)

Figure 31

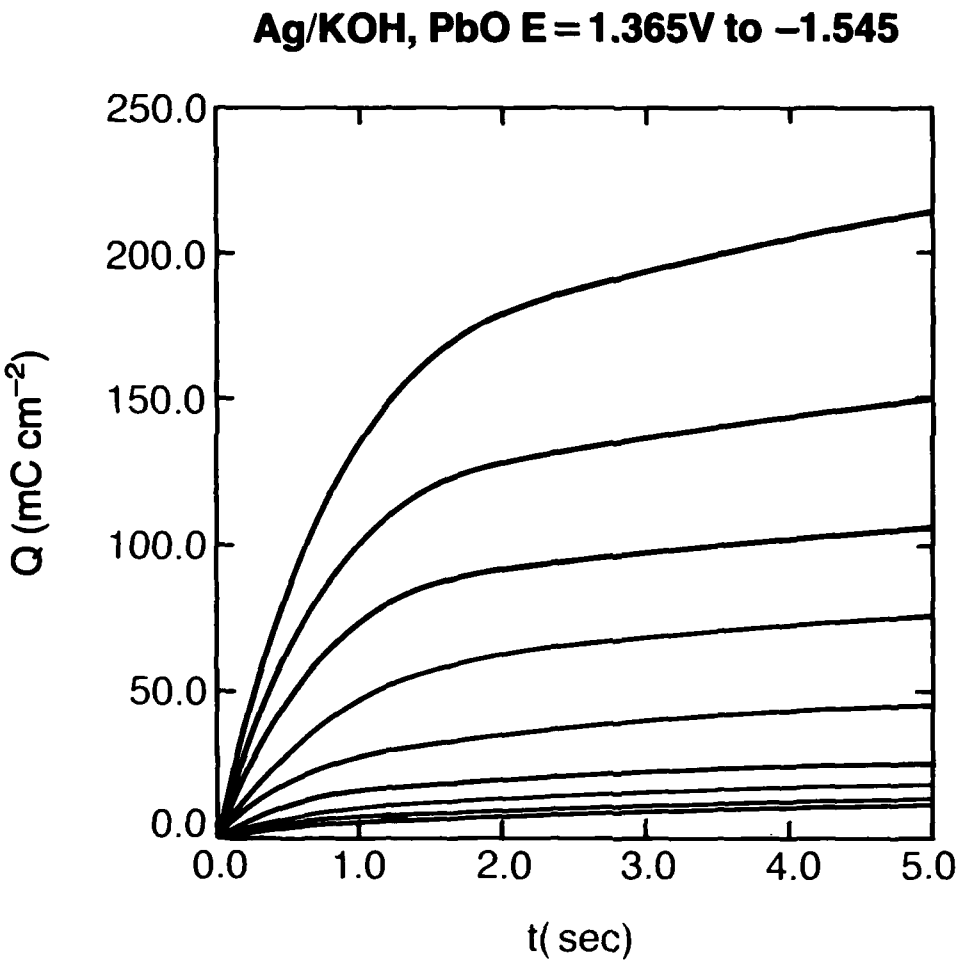
Ag/KOH, PbO E = 1.365V to −1.545
250.0
200.0
150.0
100.0
50.0
0.0
Q (mC cm^{-2})
0.0
1.0
2.0
3.0
4.0
5.0
t(sec)

Figure 32

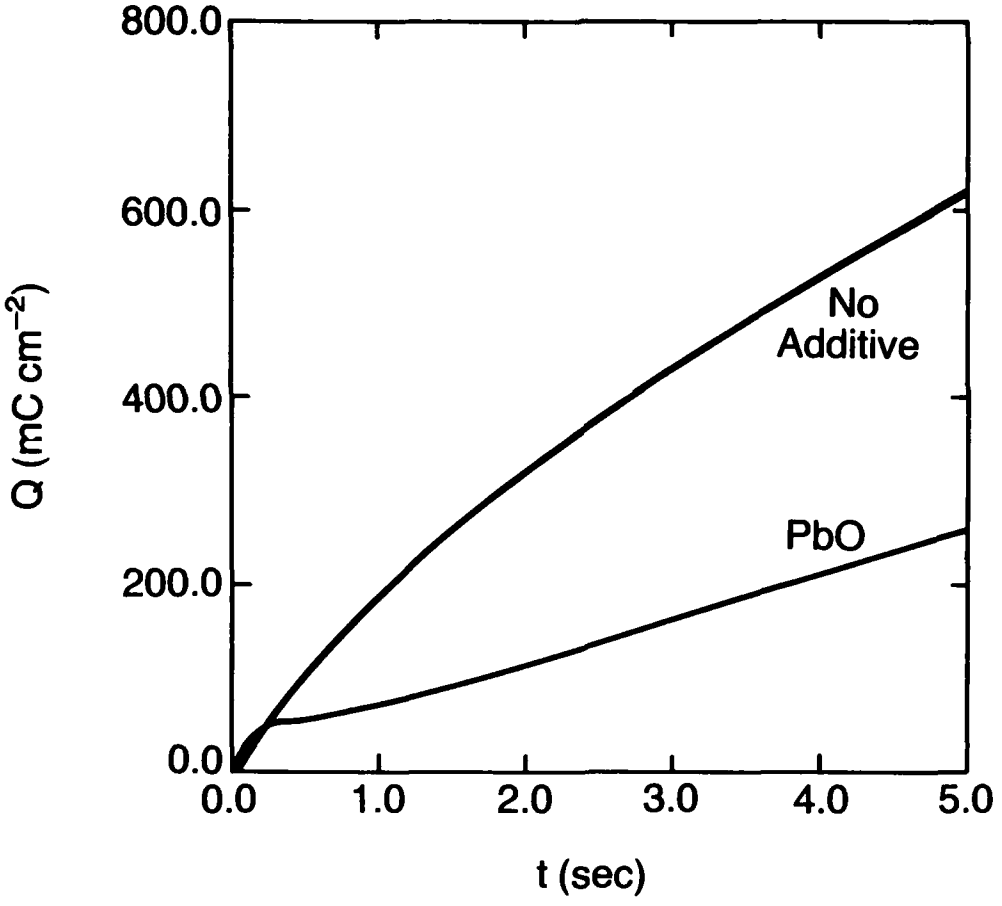
800.0
600.0
400.0
200.0
0.0
Q (mC cm^{-2})
No
Additive
PbO
0.0
1.0
2.0
3.0
4.0
5.0
t (sec)

Figure 33

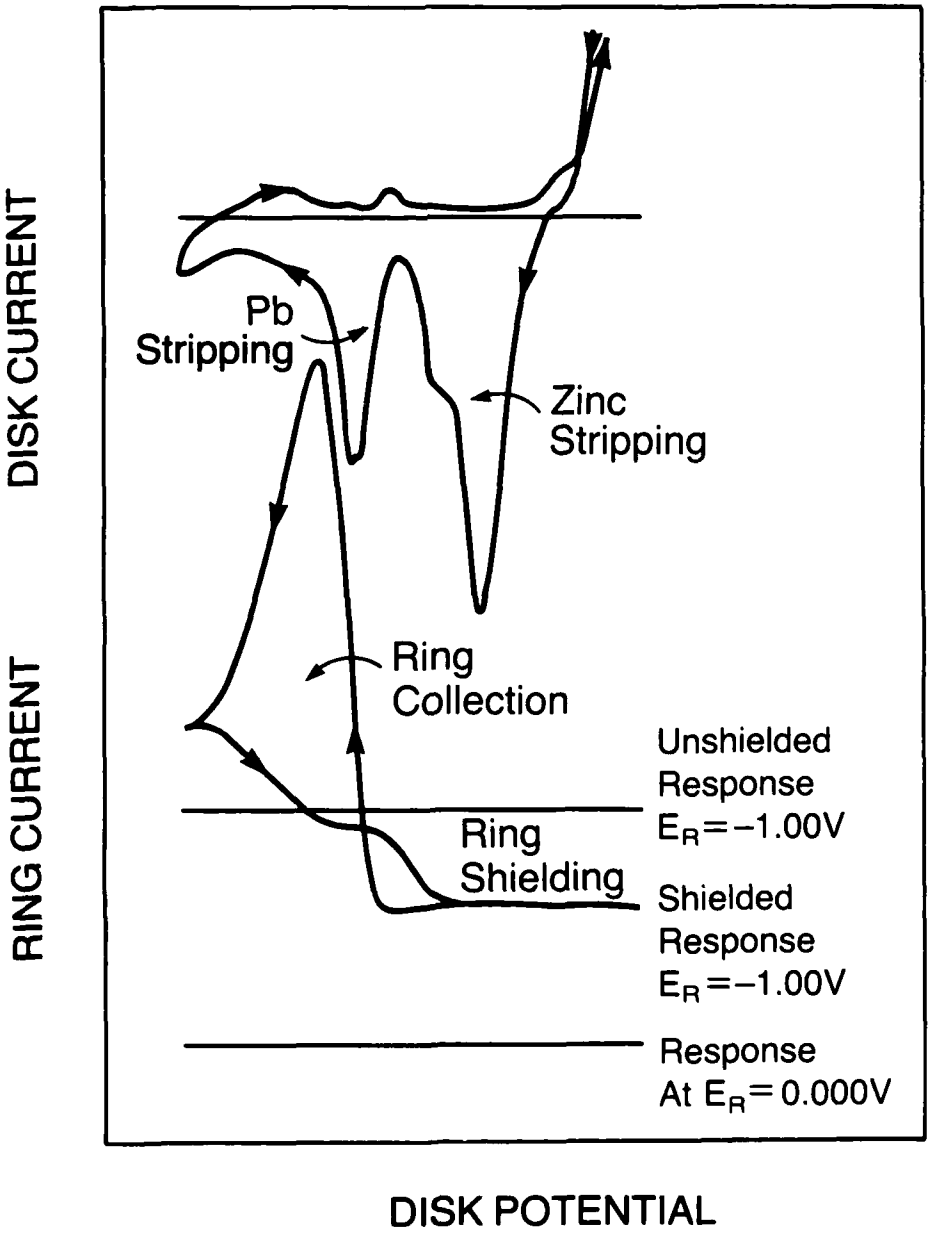
DISK CURRENT
RING CURRENT
Pb
Stripping
Zinc
Stripping
Ring
Collection
Unshielded
Response
$E_R = -1.00V$
Ring
Shielding
Shielded
Response
$E_R = -1.00V$
Response
At $E_R = 0.000V$
DISK POTENTIAL

Figure 34

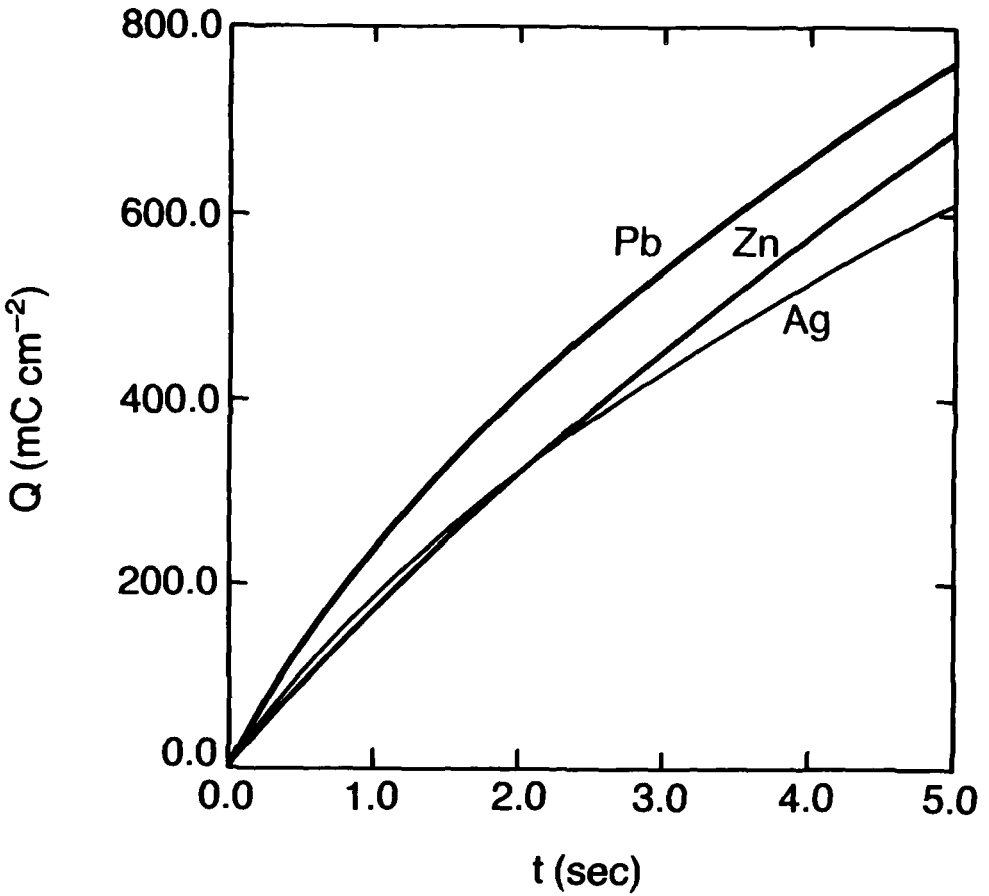

Figure 35

DL/413/83/01
GEN/413-2

TECHNICAL REPORT DISTRIBUTION LIST, GEN

	No. Copies
Office of Naval Research Attn: Code 413 800 N. Quincy Street Arlington, Virginia 22217	2
Dr. Bernard Douda Naval Weapons Support Center Code 5042 Crane, Indiana 47522	1
Commander, Naval Air Systems Command Attn: Code 310C (H. Rosenwasser) Washington, D.C. 20360	1
Naval Civil Engineering Laboratory Attn: Dr. R. W. Drisko Port Hueneme, California 93401	1
Defense Technical Information Center Building 5, Cameron Station Alexandria, Virginia 22314	12
DTNSRDC Attn: Dr. G. Bosmajian Applied Chemistry Division Annapolis, Maryland 21401	1
Dr. William Tolles Superintendent Chemistry Division, Code 6100 Naval Research Laboratory Washington, D.C. 20375	1
Dr. David Young Code 334 NORDA NSTL, Mississippi 39529	1
Naval Weapons Center Attn: Dr. Ron Atkins Chemistry Division China Lake, California 93555	1
Scientific Advisor Commandant of the Marine Corps Code RD-1 Washington, D.C. 20380	1
U.S. Army Research Office Attn: CRD-AA-IP P.O. Box 12211 Research Triangle Park, NC 27709	1
Mr. John Boyle Materials Branch Naval Ship Engineering Center Philadelphia, Pennsylvania 19112	1
Naval Ocean Systems Center Attn: Dr. S. Yamamoto Marine Sciences Division San Diego, California 91232	1

DL/413/83/01
359/413-2

ABSTRACTS DISTRIBUTION LIST, 359/627

Dr. Paul Delahay
Department of Chemistry
New York University
New York, New York 10003

Dr. P. J. Hendra
Department of Chemistry
University of Southampton
Southampton SO9 5NH
United Kingdom

Dr. J. Driscoll
Lockheed Palo Alto Research
Laboratory
3251 Hanover Street
Palo Alto, California 94304

Dr. D. N. Bennion
Department of Chemical Engineering
Brigham Young University
Provo, Utah 84602

Dr. R. A. Marcus
Department of Chemistry
California Institute of Technology
Pasadena, California 91125

Dr. J. J. Auborn
Bell Laboratories
Murray Hill, New Jersey 07974

Dr. Joseph Singer, Code 302-1
NASA-Lewis
21000 Brookpark Road
Cleveland, Ohio 44135

Dr. P. P. Schmidt
Department of Chemistry
Oakland University
Rochester, Michigan 48063

Dr. Manfred Breiter
Institut fur Technische Elektrochemie
Technischen Universitat Wien
9 Getreidemarkt, 1160 Wien
AUSTRIA

Dr. E. Yeager
Department of Chemistry
Case Western Reserve University
Cleveland, Ohio 44106

Dr. C. E. Mueller
The Electrochemistry Branch
Naval Surface Weapons Center
White Oak Laboratory
Silver Spring, Maryland 20910

Dr. Sam Perone
Chemistry & Materials
Science Department
Lawrence Livermore National Laboratory
Livermore, California 94550

Dr. Royce W. Murray
Department of Chemistry
University of North Carolina
Chapel Hill, North Carolina 27514

Dr. B. Brummer
EIC Incorporated
111 Downey Street
Norwood, Massachusetts 02062

Dr. Adam Heller
Bell Laboratories
Murray Hill, New Jersey 07974

Dr. A. B. Ellis
Chemistry Department
University of Wisconsin
Madison, Wisconsin 53706

Library
Duracell, Inc.
Burlington, Massachusetts 01803

Electrochimica Corporation
20 Kelly Court
Menlo Park, California 94025-1418

ABSTRACTS DISTRIBUTION LIST, 359/627

Dr. M. Wrighton
Chemistry Department
Massachusetts Institute
of Technology
Cambridge, Massachusetts 02139

Dr. B. Stanley Pons
Department of Chemistry
University of Utah
Salt Lake City, Utah 84112

Donald E. Mains
Naval Weapons Support Center
Electrochemical Power Sources Division
Crane, Indiana 47522

S. Ruby
DOE (STOR)
Room 5E036 Forrestal Bldg., CE-14
Washington, D.C. 20595

Dr. A. J. Bard
Department of Chemistry
University of Texas
Austin, Texas 78712

Dr. Janet Osteryoung
Department of Chemistry
State University of New York
Buffalo, New York 14214

Dr. Donald W. Ernst
Naval Surface Weapons Center
Code R-33
White Oak Laboratory
Silver Spring, Maryland 20910

Mr. James R. Moden
Naval Underwater Systems Center
Code 3632
Newport, Rhode Island 02840

Dr. Bernard Spielvogel
U.S. Army Research Office
P.O. Box 12211
Research Triangle Park, NC 27709

Dr. Aaron Fletcher
Naval Weapons Center
Code 3852
China Lake, California 93555

Dr. M. M. Nicholson
Electronics Research Center
Rockwell International
3370 Miraloma Avenue
Anaheim, California

Dr. Michael J. Weaver
Department of Chemistry
Purdue University
West Lafayette, Indiana 47907

Dr. R. David Rauh
EIC Laboratories, Inc.
111 Downey Street
Norwood, Massachusetts 02062

Dr. Aaron Wold
Department of Chemistry
Brown University
Providence, Rhode Island 02192

Dr. Martin Fleischmann
Department of Chemistry
University of Southampton
Southampton SO9 5NH ENGLAND

Dr. R. A. Osteryoung
Department of Chemistry
State University of New York
Buffalo, New York 14214

Dr. John Wilkes
Air Force Office of Scientific
Research
Bolling AFB
Washington, D.C. 20332

Dr. R. Nowak
Naval Research Laboratory
Code 6171
Washington, D.C. 20375

Dr. D. F. Shriver
Department of Chemistry
Northwestern University
Evanston, Illinois 60201

ABSTRACTS DISTRIBUTION LIST, 359/627

Dr. Hector D. Abruna
Department of Chemistry
Cornell University
Ithaca, New York 14853

Dr. A. B. P. Lever
Chemistry Department
York University
Downsview, Ontario M3J1P3

Dr. Stanislaw Szpak
Naval Ocean Systems Center
Code 633, Bayside
San Diego, California 95152

Dr. Gregory Farrington
Department of Materials Science
and Engineering
University of Pennsylvania
Philadelphia, Pennsylvania 19104

M. L. Robertson
Manager, Electrochemical
and Power Sources Division
Naval Weapons Support Center
Crane, Indiana 47522

Dr. T. Marks
Department of Chemistry
Northwestern University
Evanston, Illinois 60201

Dr. Micha Tomkiewicz
Department of Physics
Brooklyn College
Brooklyn, New York 11210

Dr. Lesser Blum
Department of Physics
University of Puerto Rico
Rio Piedras, Puerto Rico 00931

Dr. Joseph Gordon, II
IBM Corporation
5600 Cottle Road
San Jose, California 95193

Dr. Nathan Lewis
Department of Chemistry
Stanford University
Stanford, California 94305

Dr. D. H. Whitmore
Department of Materials Science
Northwestern University
Evanston, Illinois 60201

Dr. Alan Bewick
Department of Chemistry
The University of Southampton
Southampton, SO9 5NH ENGLAND

Dr. E. Anderson
NAVSEA-56Z33 NC #4
2541 Jefferson Davis Highway
Arlington, Virginia 20362

Dr. Bruce Dunn
Department of Engineering &
Applied Science
University of California
Los Angeles, California 90024

Dr. Elton Cairns
Energy & Environment Division
Lawrence Berkeley Laboratory
University of California
Berkeley, California 94720

Dr. Richard Pollard
Department of Chemical Engineering
University of Houston
Houston, Texas 77004

Dr. M. Philpott
IBM Corporation
5600 Cottle Road
San Jose, California 95193

Dr. Donald Sandstrom
Boeing Aerospace Co.
P.O. Box 3999
Seattle, Washington 98124

Dr. Carl Kannewurf
Department of Electrical Engineering
and Computer Science
Northwestern University
Evanston, Illinois 60201

Dr. Joel Harris
Department of Chemistry
University of Utah
Salt Lake City, Utah 84112

ABSTRACTS DISTRIBUTION LIST, 359/627

Dr. Robert Somoano
Jet Propulsion Laboratory
California Institute of Technology
Pasadena, California 91103

Dr. Johann A. Joebstl
USA Mobility Equipment R&D Command
DRDME-EC
Fort Belvoir, Virginia 22060

Dr. Judith H. Ambrus
NASA Headquarters
M.S. RTS-6
Washington, D.C. 20546

Dr. Albert R. Landgrebe
U.S. Department of Energy
M.S. 6B025 Forrestal Building
Washington, D.C. 20595

Dr. J. J. Brophy
Department of Physics
University of Utah
Salt Lake City, Utah 84112

Dr. Charles Martin
Department of Chemistry
Texas A&M University
College Station, Texas 77843

Dr. H. Tachikawa
Department of Chemistry
Jackson State University
Jackson, Mississippi 39217

Dr. Theodore Beck
Electrochemical Technology Corp.
3935 Leary Way N.W.
Seattle, Washington 98107

Dr. Farrell Lytle
Boeing Engineering and
Construction Engineers
P.O. Box 3707
Seattle, Washington 98124

Dr. Robert Gotscholl
U.S. Department of Energy
MS G-226
Washington, D.C. 20545

Dr. Edward Fletcher
Department of Mechanical Engineering
University of Minnesota
Minneapolis, Minnesota 55455

Dr. John Fontanella
Department of Physics
U.S. Naval Academy
Annapolis, Maryland 21402

Dr. Martha Greenblatt
Department of Chemistry
Rutgers University
New Brunswick, New Jersey 08903

Dr. John Wasson
Syntheco, Inc.
Rte 6 - Industrial Pike Road
Gastonia, North Carolina 28052

Dr. Walter Roth
Department of Physics
State University of New York
Albany, New York 12222

Dr. Anthony Sammells
Eltron Research Inc.
4260 Westbrook Drive, Suite 111
Aurora, Illinois 60505

Dr. C. A. Angell
Department of Chemistry
Purdue University
West Lafayette, Indiana 47907

Dr. Thomas Davis
Polymer Science and Standards
Division
National Bureau of Standards
Washington, D.C. 20234

Ms. Wendy Parkhurst
Naval Surface Weapons Center R-33
R-33
Silver Spring, Maryland 20910

DL/413/83/01
359/413-2

ABSTRACTS DISTRIBUTION LIST, 359/627

Dr. John Owen
Department of Chemistry and
Applied Chemistry
University of Salford
Salford M5 4WT ENGLAND

Dr. Boone Owens
Department of Chemical Engineering
and Materials Science
University of Minnesota
Minneapolis, Minnesota 55455

Dr. J. O. Thomas
University of Uppsala
Institute of Chemistry
Box 531
S-751 21 Uppsala, Sweden

Dr. O. Stafsudd
Department of Electrical Engineering
University of California
Los Angeles, California 90024

Dr. S. G. Greenbaum
Department of Physics
Hunter College of CUNY
New York, New York 10021

Dr. Menahem Anderman
W.R. Grace & Co.
Columbia, Maryland 20144

END

FILMED

10-85

DTIC